

Article

Design, Synthesis and Characterization of Benzimidazole Derivatives as PET Imaging Ligands for Metabotropic Glutamate Receptor 2 (mGluR2)

Gengyang Yuan, Xiyang Qu, baohui Zheng, Ramesh Neelamegam, Sepideh Afshar, Suhasini Iyengar, Chuzhi Pan, Junfeng Wang, Hye Jin Kang, Mary Jo Ondrechen, Pekka Poutiainen, Georges El Fakhri, Zhaoda Zhang, and Anna-Liisa Brownell

J. Med. Chem., **Just Accepted Manuscript** • DOI: 10.1021/acs.jmedchem.0c01394 • Publication Date (Web): 28 Sep 2020

Downloaded from pubs.acs.org on October 4, 2020

Just Accepted

“Just Accepted” manuscripts have been peer-reviewed and accepted for publication. They are posted online prior to technical editing, formatting for publication and author proofing. The American Chemical Society provides “Just Accepted” as a service to the research community to expedite the dissemination of scientific material as soon as possible after acceptance. “Just Accepted” manuscripts appear in full in PDF format accompanied by an HTML abstract. “Just Accepted” manuscripts have been fully peer reviewed, but should not be considered the official version of record. They are citable by the Digital Object Identifier (DOI®). “Just Accepted” is an optional service offered to authors. Therefore, the “Just Accepted” Web site may not include all articles that will be published in the journal. After a manuscript is technically edited and formatted, it will be removed from the “Just Accepted” Web site and published as an ASAP article. Note that technical editing may introduce minor changes to the manuscript text and/or graphics which could affect content, and all legal disclaimers and ethical guidelines that apply to the journal pertain. ACS cannot be held responsible for errors or consequences arising from the use of information contained in these “Just Accepted” manuscripts.

1
2
3 **Design, Synthesis and Characterization of Benzimidazole Derivatives as PET Imaging**
4
5 **Ligands for Metabotropic Glutamate Receptor 2 (mGluR2)**
6
7
8
9

10 Gengyang Yuan,^{†,#,*} Xiying Qu,^{†,#} Baohui Zheng,[†] Ramesh Neelamegam,[†] Sepideh Afshar,[†]
11 Suhasini Iyengar,[‡] Chuzhi Pan,[†] Junfeng Wang,[†] Hye Jin Kang,^{||} Mary Jo Ondrechen,[‡] Pekka
12 Poutiainen,[⊥] Georges El Fakhri,[†] Zhaoda Zhang,^{§,*} and Anna-Liisa Brownell^{†,*}
13
14
15
16
17
18

19 [†]Gordon Center for Medical Imaging, Massachusetts General Hospital and Harvard Medical
20 School, 3rd Avenue, Charlestown, MA 02129, USA
21
22

23 [‡]Department of Chemistry and Chemical Biology, Northeastern University, 360 Huntington
24 Avenue, Boston, MA 02115, USA
25
26

27 [§]Athinoula A. Martinos Center for Biomedical Imaging, Massachusetts General Hospital and
28 Harvard Medical School, 149 Thirteenth Street, Suite 2301 Charlestown, MA 02129, USA
29
30

31 ^{||}Department of Pharmacology, University of North Carolina Chapel Hill School of Medicine,
32 Chapel Hill, NC 27514, USA
33
34

35 [⊥]Department of Clinical Physiology and Nuclear Medicine, Kuopio University Hospital, Kuopio,
36 70210, Finland
37
38

39 [#]Equal effort
40
41
42
43
44
45
46
47
48
49
50
51
52
53
54
55
56
57
58
59
60

ABSTRACT: Three benzimidazole derivatives (**13-15**) have been synthesized as potential PET imaging ligands for mGluR2 in the brain. Of these compounds, **13** exhibits potent binding affinity ($IC_{50} = 7.6 \pm 0.9$ nM), PAM activity ($EC_{50} = 51.2$ nM), and excellent selectivity against other mGluR subtypes (> 100 -fold). [^{11}C]**13** was synthesized via *O*-[^{11}C]methylation of its phenol precursor **25** with [^{11}C]methyl iodide. The achieved radiochemical yield was $20 \pm 2\%$ ($n = 10$, decay-corrected) based on [^{11}C]CO₂ with radiochemical purity $> 98\%$ and molar activity 98 ± 30 GBq/ μ mol EOS. *Ex vivo* biodistribution studies revealed reversible accumulation of [^{11}C]**13** and hepatobiliary and urinary excretions. PET imaging studies in rats demonstrated that [^{11}C]**13** accumulated in the mGluR2-rich brain regions. Pre-administration of mGluR2-selective PAM, **17** reduced the brain uptake of [^{11}C]**13**, indicating a selective binding. Therefore, [^{11}C]**13** is a potential PET imaging ligand for mGluR2 in different CNS related conditions.

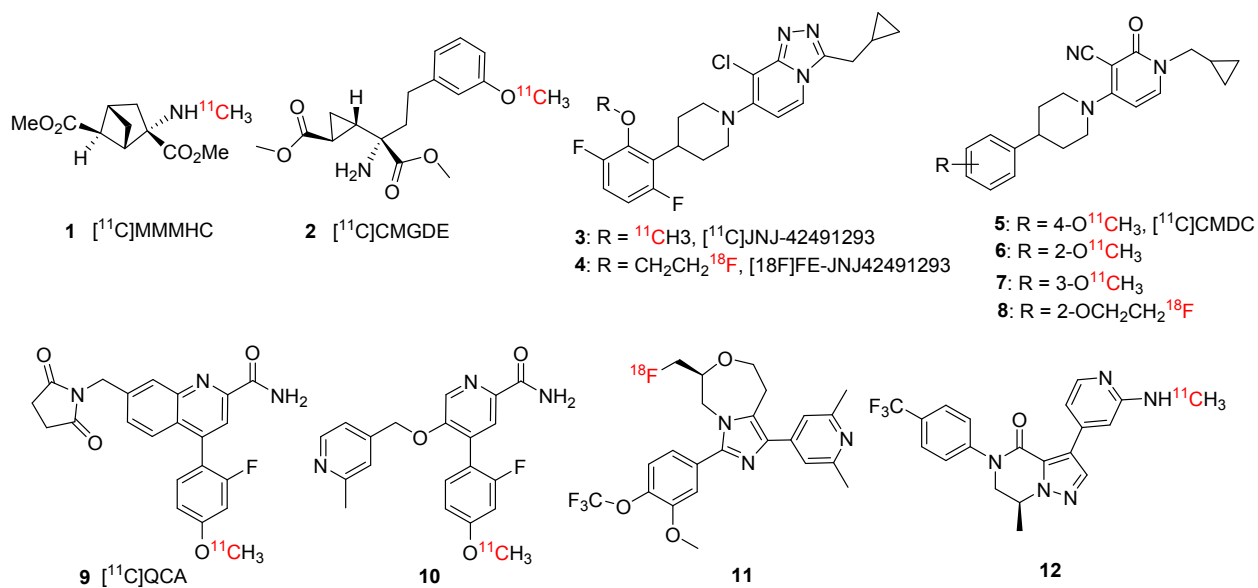
INTRODUCTION

The metabotropic glutamate receptor 2 (mGluR2) is widely expressed in the nervous systems.^{1,2} mGluR2 expression is abundant in brain areas such as prefrontal cortex, hippocampus, amygdala, striatum, thalamus, cerebellum, and nucleus accumbens.^{3,4} It predominantly localizes on presynaptic nerve terminals and modulates synaptic transmission and neuroplasticity.³ Structurally, mGluR2 has a characteristic extracellular Venus flytrap domain (VFTD), a seven transmembrane (7-TM) domain and a cysteine rich domain (CRD) that connects the mGluR dimers.⁵ The therapeutic benefits of mGluR2 modulators have been suggested for Alzheimer's disease⁶⁻⁹, schizophrenia¹⁰⁻¹³, depression¹⁴, anxiety¹⁵ and pain¹⁶⁻¹⁸.

1
2
3 Initial research and drug discovery efforts had focused on pharmacological ligands for
4 mGluR2/3, which have been published in literature and developed for the treatment of anxiety and
5 schizophrenia in preclinical and clinical studies.^{10-13,15} Until recently, mGluR2 and mGluR3 have
6
7 been thought to have similar functions: they share high sequence homology, generally couple to
8 Gi/o signaling, and provide negative feedback to reduce glutamate signaling. However, despite a
9
10 successful phase 2 study conducted entirely in Russia for patients with schizophrenia, the clinical
11 development of LY2140023, a mGluR2/3 receptor agonist prodrug, was halted due to lack of
12
13 antipsychotic efficacy compared to placebo in three phase 2 or phase 3 trials.^{12,19-21} The studies
14
15 also revealed that the antipsychotic effect of mGluR2/3 agonists was absent in mGluR2 knockout
16
17 mice but not mGluR3 knockout mice, suggesting the antipsychotic effects might be mediated via
18
19 the mGlu2 but not mGlu3 receptor and even the effect of mGluR2 and mGluR3 might be
20
21 different/opposite.^{22,23}

22
23
24
25
26
27
28
29
30
31 Previously, we have reported two orthosteric antagonists as PET tracers, namely,
32
33 [¹¹C]MMMHC (**1**) in 2003²⁴ and [¹¹C]CMGDE (**2**) in 2012²⁵, for Group II mGluRs (mGluR2 &
34
35 mGluR3) (Figure 1). Since then, several PET radiotracers for mGluR2 have been derived from
36
37 allosteric modulators that target the 7-TM instead of the VFTD region of mGluR2. It is believed
38
39 that the allosteric modulators would bear higher lipophilicity and mGluR2 selectivity than
40
41 orthosteric ligands due to the hydrophobicity and heterogeneity of the 7-TM binding pocket across
42
43 mGlu receptors.²⁶⁻²⁸ So far, two radioligands in this category have been advanced for human
44
45 clinical trials, including mGluR2 PAM [¹¹C]JNJ42491293 (**3**) and a radioligand from Merck.
46
47 However, [¹¹C]JNJ42491293 (**3**) was not found useful for the visualization and quantification of
48
49 mGluR2 *in vivo* because of its apparent off-target binding.^{29,30} The Merck radiotracer was only
50
51 reported in an abstract without information on its chemical structure and detailed imaging
52
53
54
55
56
57
58
59
60

1
2
3 results.^{31,32} The fluorine-18 labeled derivative of **3**, [¹⁸F]FE-JNJ-42491293 (**4**), was disclosed in
4
5 an abstract but it is not clear if this tracer has the similar off-target binding as **3**.³³ Recently, a
6
7 mGluR2 PAM tracer [¹¹C]CMDC (**5**) and its three derivatives **6-8** were reported; however, **5**
8
9 exhibited an insufficient affinity and low BBB-penetration. PET imaging with **5** did not enable *in*
10
11 *vivo* visualization of the living rat brain.^{34,35} On the other hand, three different types of mGluR2
12
13 NAM-based tracers were also disclosed. The mGluR2 NAM tracers [¹¹C]QCA (**9**)³⁶ and its
14
15 analogue [¹¹C]**10**³⁷ showed off-target binding and limited brain uptake with intensive interaction
16
17 with brain efflux pumps on the murine BBB. Two other types of NAM-based radiotracers have
18
19 been disclosed in the patent literature. The compound **11** and its derivatives were patented as PET
20
21 tracers for mGluR2/3.³⁸ The compound **12** and its derivatives were developed as mGluR2 PET
22
23 ligands, but no *in vivo* PET imaging result has been described.³⁹
24
25
26
27
28
29
30



50
51 **Figure 1.** Typical PET radiotracers for mGluR2.
52
53
54
55
56
57
58
59
60

The lack of efficient and efficacious mGluR2 PET tracers prompted us to further extend our previous effort toward exploration of mGluR2 PAMs as suitable PET imaging candidates. The benzimidazole derivatives have been the most widely examined series of mGluR2 PAMs in literature^{27,40,41} with examples of highly potent mGluR2 ligands of compounds **13** ($EC_{50} = 13$ nM)⁴² and **14** ($EC_{50} = 5$ nM, Figure 2)⁴¹. The presence of 2-methoxy-4-trifluoromethyl-phenyl group in compounds **13** and **14** allows rapid radiolabeling of their phenol precursors via *O*-¹¹C methylation with [¹¹C]CH₃I. We further designed compound **15** as a PET imaging candidate based on a potent mGluR2 PAM [2-(((1*R*,5*S*,6*r*)-6-((4-chloro-2-fluorophenoxy)methyl)-3-azabicyclo[3.1.0]hexan-3-yl)methyl)-1-methyl-1*H*-benzo[*d*]imidazole] (**16**, $EC_{50} = 8$ nM)⁴³ by replacing the distal 4-chloro-2-fluorophenoxy group with a 2-methoxy-4-(trifluoromethyl)phenoxy moiety. The structurally distinct compound **17**, a potent and selective mGluR2 PAM ($EC_{50} = 78$ nM),⁴⁴ was used as a selective blocking reagent during the investigation of [¹¹C]JNJ42491293 (**3**) and therefore we used it as a blocking reagent in the present studies.³⁰ Here, we report the design, synthesis and characterization of compounds **13-15** using *in silico* modeling, *in vitro* assays and *in vivo* PET imaging methods to evaluate their potential as mGluR2-selective PET imaging ligands.

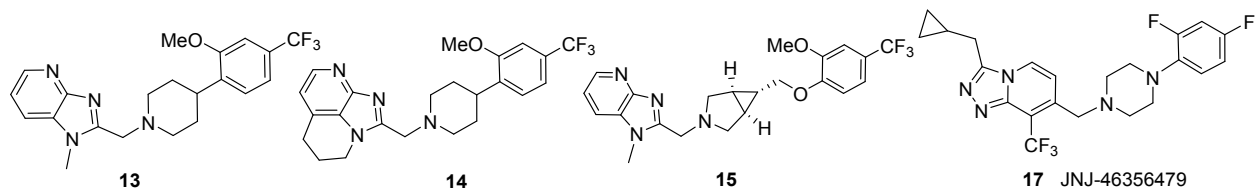
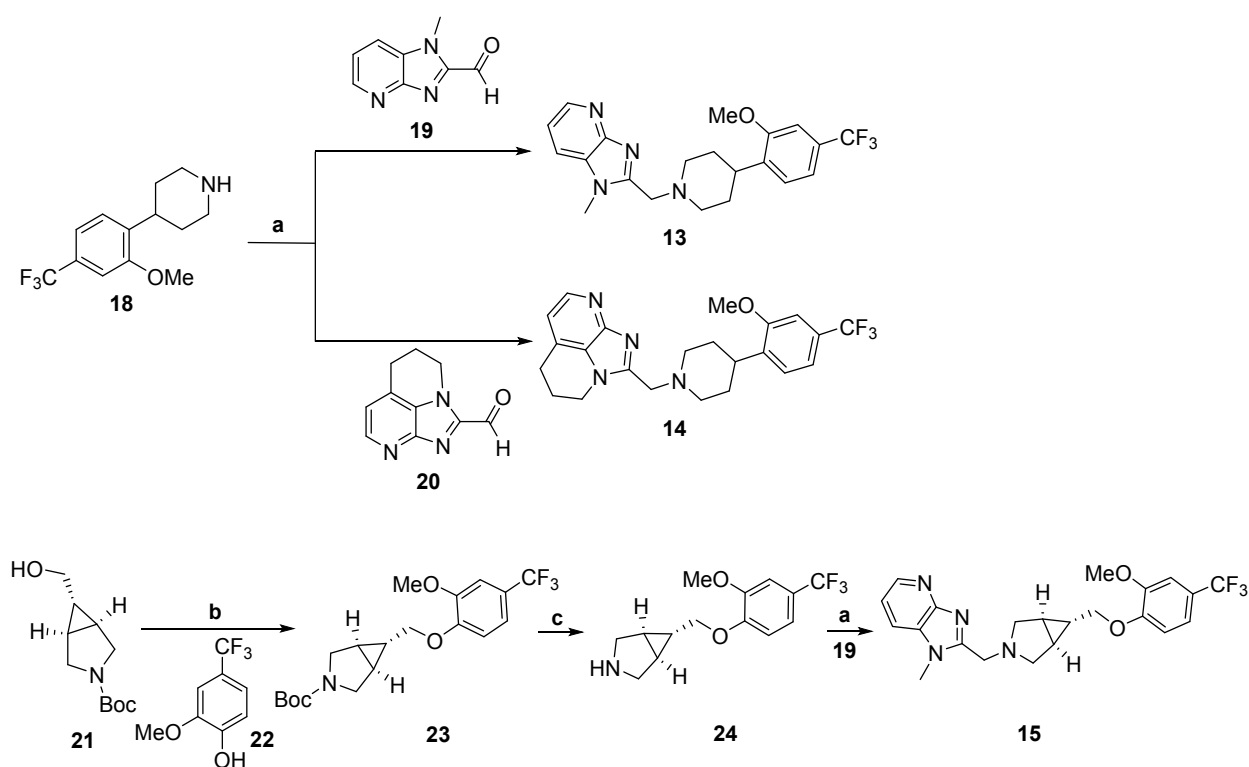


Figure 2. Chemical structures of compounds **13-15** and **17**.

RESULTS AND DISCUSSION

Chemistry. Structurally, compounds **13-15** feature a merged heterocyclic core, a central cyclic amine core and a substituted distal arene. These compounds were synthesized according to reaction sequences delineated in Scheme 1. The intermediates **18-20** were prepared according to the reported procedures.^{41,42} The intermediate **24** was synthesized in two steps: Mitsunobu reaction of **21** and **22**; followed by removal of N-Boc-group. Finally, compounds **13-15** were synthesized by the corresponding reductive amination reactions. Compound **17** was prepared according to the published procedure.⁴⁴



Scheme 1. Syntheses of **13-15**. Reagents and conditions: (a) Et₃N, MgSO₄, then Na(OAc)₃BH, DCE, rt, overnight; (b) PPh₃, diethyl azodicarboxylate solution (40 wt.% in toluene), THF, rt, 16 h; (c) TFA, DCM, rt, 2 h.

1
2
3 **Structural insights of compounds 13-15.** To provide structural insights on ligand-protein binding,
4 compounds **13-15** were docked into a mGluR2 homology model, which was the best of 15 models
5
6 built in YASARA⁴⁵ (Supporting Information Figure S1 and Table S1). The best model is a hybrid
7
8 model based on three structures, an mGluR1 structure from rat (PDB ID 1EWK)⁴⁶ and two human
9
10 mGluR5 structures (PDB IDs 3LMK⁴⁷ and 6N52⁴⁸). This model was validated by a series of
11
12 structural analysis tools of ModFOLD⁴⁹, ERRAT and VERIFY 3D⁵⁰⁻⁵² (see Supporting
13
14 Information Figures S2-S7) and used for the docking studies. The key binding residues were
15
16 predicted by Partial Order Optimum Likelihood (POOL)⁵³, DEPTH⁵⁴ and MetaPocket⁵⁵
17
18 (Supporting Information Figure S8). The docking experiments were performed at the 7-TM region
19
20 with AutoDock embedded in YASARA (Supporting Information Table S2).⁵⁶ As shown in Figure
21
22 3, compounds **13-15** would localize similarly at the entrance of the 7-TM region with their
23
24 heterocyclic cores projecting to the bottom hydrophobic pocket and the distal substituted arenes
25
26 interacting with residues at the extracellular loop 2 (EL2). Compounds **13** and **14** have the best
27
28 docking scores of 8.7 kcal/mol and 8.6 kcal/mol, respectively, compared to the value of 7.3
29
30 kcal/mol for compound **15**. Compound **13** shows a hydrogen bonding interaction with Arg788, a
31
32 π -cation interaction with Arg720, and a π - π stacking interaction with His723 (Figure 3). His723
33
34 has been previously reported as a key hydrophobic residue that interacts with several mGluR2
35
36 PAMs.^{57,58} Compound **14** has similar key binding interactions as that of compound **13**, whereas,
37
38 compound **15** exhibited fewer contacts in the binding pocket than compounds **13** and **14**, consistent
39
40 with the decreased docking score. Overall, the *in silico* simulations suggest compounds **13-15** as
41
42 potent mGluR2 binding ligands.
43
44
45
46
47
48
49
50
51
52
53

54 (a)

(b)

(c)

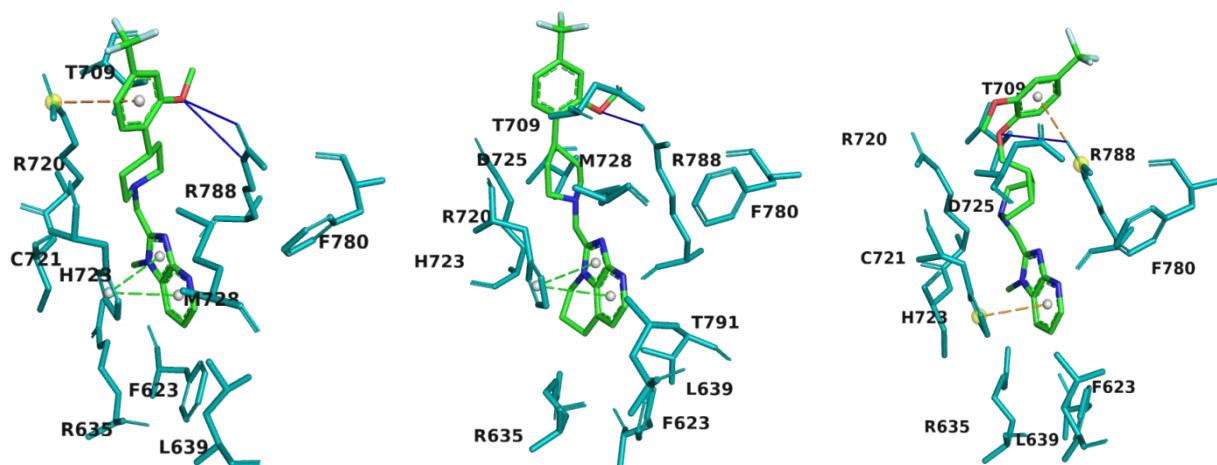


Figure 3. Snapshots of the docking results for compounds **13** (a), **14** (b) and **15** (c). Pictures were rendered in PyMol 2.3.3. The interacting residues are shown in teal. The ligand atoms are rendered as carbon in green, nitrogen in blue, oxygen in red, and fluorine in cyan. Blue lines represent H-bonds, green dotted lines show π - π stacking, and orange dotted lines indicate π -cation interaction. Structure is based on a hybrid model built from PDB structures of 1EWK⁴⁶, 3LMK⁴⁷, and 6N52⁴⁸.

***In vitro* properties.** To evaluate compounds **13-15**, the pharmacological and physicochemical properties including affinity to mGluR2, mGluR2 PAM activity, selectivity toward other mGluRs, lipophilicity, plasma protein binding (PPB), metabolic and solution stabilities as well as blood brain barrier (BBB) penetration capability were determined. In these studies, compound **13** was compared to the other two mGluR2 ligands **14** and **15**.

The binding affinity of compounds **13-15** was measured by the competitive binding assay in mGluR2 transfected CHO cells at the presence of 10 nM tritium-labeled radioligand [³H]JNJ-46281222 (see Supporting Information).⁵⁹⁻⁶¹ The concentration of compounds **13-15** was increased from 0.01 nM to 10 μ M to generate a competitive binding curve, with which the IC₅₀ values were determined. As displayed in Table 1, compound **13** has potent binding toward mGluR2 (IC₅₀ = 7.6

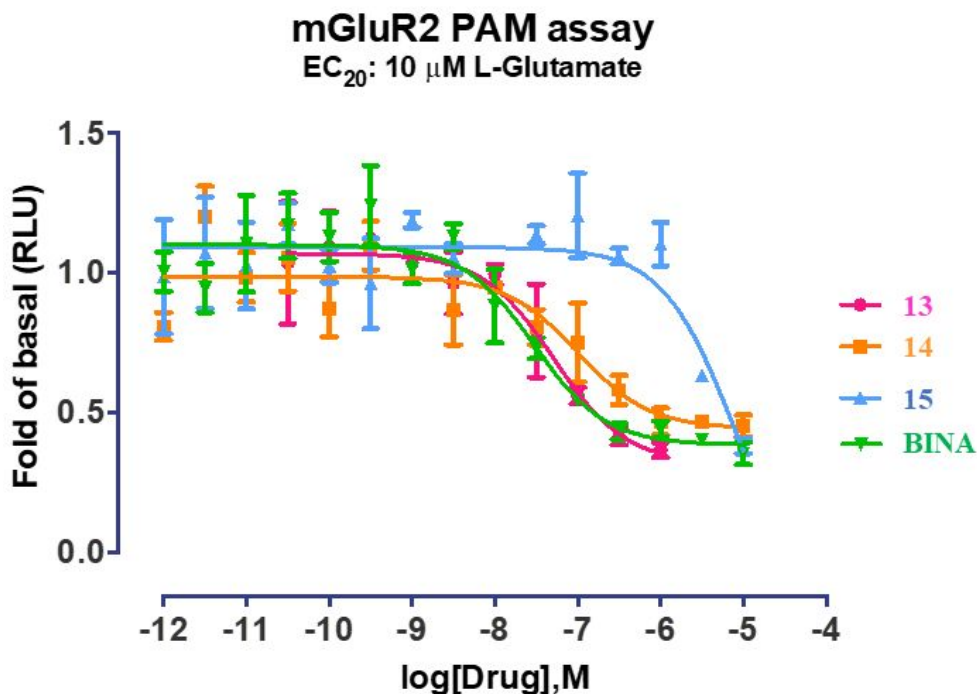
± 0.9 nM), which is slightly stronger than those of compounds **14** ($IC_{50} = 10.5 \pm 0.5$ nM) and **15** ($IC_{50} = 10.5 \pm 7.9$ nM). Even the results were consistent, they do not yet prove the same allosteric binding site at mGluR2 for all these ligands.

Table 1. Binding inhibition assay of compounds **13-15** to mGluR2.

Compound	13	14	15
$IC_{50} \pm SEM$ (nM)	7.6 ± 0.9	10.5 ± 0.5	10.5 ± 7.9
$\log(IC_{50} \pm SEM)$	-8.12 ± 0.79	-7.98 ± 0.21	-7.98 ± 1.39

Previously reported EC_{50} values for compounds **13** and **14** ($EC_{50} = 13$ nM and 5 nM, respectively)^{41,42} were determined by forced-coupling of mGluR2 to $G_{\alpha_{15}}$ or $G_{\alpha_{16}}$ followed by fluorescence detection of calcium flux upon activation. However, this assay is sub-optimal as it does not signal through the biorelevant cAMP pathway. Here, the mGluR2 PAM activity of compounds **13-15** was determined using Promega's split luciferase based GloSensor cAMP biosensor assay,^{62,63} where, with this live cell assay, the mGluR2 PAM activity was evaluated in the presence of EC_{20} amount of L-glutamate by measuring changes in intracellular cAMP concentration, the relevant second messenger mechanism. An mGluR2 PAM, [3'-(((2-cyclopentyl-6,7-dimethyl-1-oxo-2,3-dihydro-1*H*-inden-5-yl)oxy)methyl)-[1,1'-biphenyl]-4-carboxylic acid] (BINA),⁶⁴ was used as the reference compound for the assay. As Figure 4 shows, the EC_{50} values of **13**, **14** and **15** are 51.2 nM, 101 nM and 7.8 μ M, respectively, suggesting that **13** is a very potent mGluR2 PAM. The selectivity of **13-15** was also analyzed among the various mGluR subtypes, in which the G_q coupled receptors (mGluR1 and mGluR5) were tested using Ca^{2+} mobilization assay and the $G_{i/o}$ coupled receptors (mGluR2, mGluR3, mGluR4, mGluR6 and mGluR8) using cAMP

assay. Results demonstrate that **13** has good selectivity against other mGlu receptors (> 100-fold, Supporting Information Table S3).



Compound	13	14	15	BINA
EC ₅₀	5.12E-08	1.01E-07	7.81E-06	2.97E-08

Figure 4. mGluR2 PAM activity of compounds **13-15** was determined using Promega's split luciferase based GloSensor cAMP. The EC₅₀ values of **13**, **14** and **15** are 51.2 nM, 101 nM and 7.8 μM, respectively, suggesting that **13** is a very potent mGluR2 PAM

The *in silico* physicochemical properties of compounds **13-15** were calculated via ChemBiodraw (version 16.0) based on the molecular weight (MW), topological polar surface area (tPSA), and cLogP (Table 2). The experimental lipophilicity was measured by using reversed-phase HPLC method.⁶⁵ The LogP values obtained for compounds **13-15** were 3.65, 3.86 and 3.30

1
2
3 respectively, indicating their satisfactory CNS penetrating potentials (Supporting Information
4 Table S5).⁶⁶ The plasma protein binding comprises compounds' binding to albumin, α 1-acid
5 glycoprotein and lipoproteins once delivered to the bloodstream. This property was evaluated for
6 compounds **13** and **14** by equilibrium dialysis,⁶⁷ where two chambers were separated by a dialysis
7 membrane (MWCO 8 kD). The plasma protein bindings of **13** and **14** are 87.2% and 88.7%,
8 respectively (Supporting Information Tables 1 and S6). Therefore, the high plasma free fraction
9 of compounds **13** and **14** (> 10%) would allow enough free drug concentration in blood stream to
10 reach the brain targets.
11
12
13
14
15
16
17
18
19
20
21
22
23

24 **Table 2.** Physicochemical properties of compounds **13-15**

Compound	MW (g/mol)	tPSA (\AA^2)	HBD	cLogP	Log P	PPB \pm SEM (%)
13	404.44	40.43	1	3.57	3.65	87.2 \pm 0.1
14	430.48	40.43	1	4.08	3.86	88.7 \pm 0.1
15	432.45	49.66	1	2.89	3.3	---

26
27
28
29
30
31
32
33
34 The *in vitro* plasma and liver microsomal stability of **13** and **14** were studied by incubating the
35 test compounds in rat serum and rat liver microsomes as well as NADPH cofactor, respectively,
36 using previously published methods.^{68,69} Diltiazem and ML128 (a mGluR4 PAM)^{70,71} were used
37 as co-assay QC controls for plasma and microsomal stability assays, respectively, to ensure that
38 the assays were operating properly, and that the activity of the plasma and microsomes were
39 consistent with established criteria. Compounds **13** and **14** are much more stable than diltiazem in
40 rat plasma (Supporting Information Tables 3 and S7). The results also show that **13** and **14** exhibit
41 reasonable microsomal stability and are much more stable than ML128, in which the suitable
42 hepatic clearance of **13** and **14** is predicted (Supporting Information Tables 2 and S8-S9). The
43 solution stability of **13** was evaluated with buffer solutions at pH 5.0, 7.4 and 9.4, respectively
44
45
46
47
48
49
50
51
52
53
54
55
56
57
58
59
60

(Supporting Information Tables 3 and S10).⁷² The results indicate that **13** is relatively stable in pH ranging from 5.0 to 9.4.

Table 3. The *in vitro* stability of compounds **13-15**

Compound	The plasma stability	The microsome stability		The solution stability		
	The intact \pm SEM at 120 min (%)	$t_{1/2}$ (min)	CL _{int} (μ L/min/mg protein)	The intact \pm SEM at 120 min (%)		
				pH = 5.0	pH = 7.4	pH = 9.4
13	96.6 \pm 2.1	74.5	17.9	95.3 \pm 0.3	94.5 \pm 0.4	96.1 \pm 0.7
14	89.2 \pm 0.6	73.7	18.1	---	---	---
Diltiazem	43.2 \pm 0.8	---	---	---	---	---
ML128	---	4.2	317.1	---	---	---

BBB penetration was a major barrier for some recently reported mGluR2 PET tracers that otherwise could have efficacy for imaging the brain target as shown by radiotracers [¹¹C]**9** and [¹¹C]**10**.^{36,37} We have studied BBB penetration potential of compounds **13-15** with two *in vitro* assays, namely, parallel artificial membrane permeability assay (PAMPA) and Pgp-GloTM assay. The PAMPA assay was carried out to predict passive BBB permeability.⁷³ Quality control standards were run with each sample set to monitor the consistency of the analysis. Verapamil was used as a high permeability standard ($P_e = 16 \times 10^{-6}$ cm/s) and theophylline was used as a low permeability standard ($P_e = 0.12 \times 10^{-6}$ cm/s). As Figure 5a shows, compound **13** has the best membrane permeability with an average effective permeability (P_e) value of 9.3×10^{-6} cm/s.

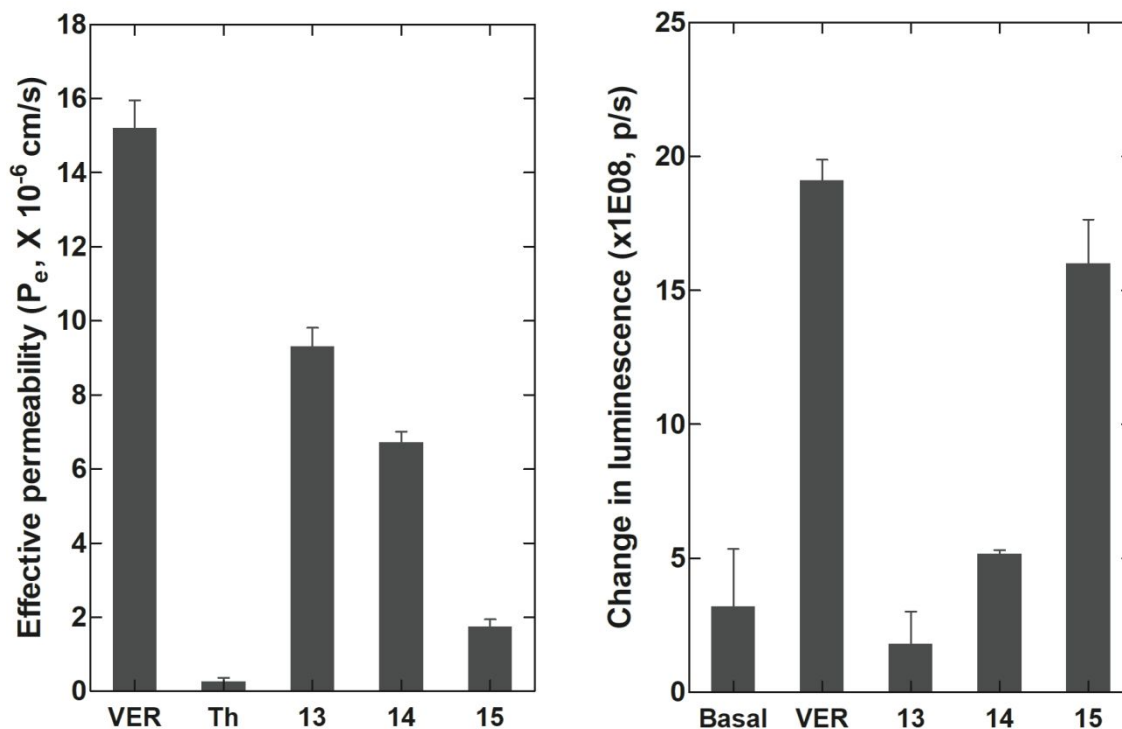
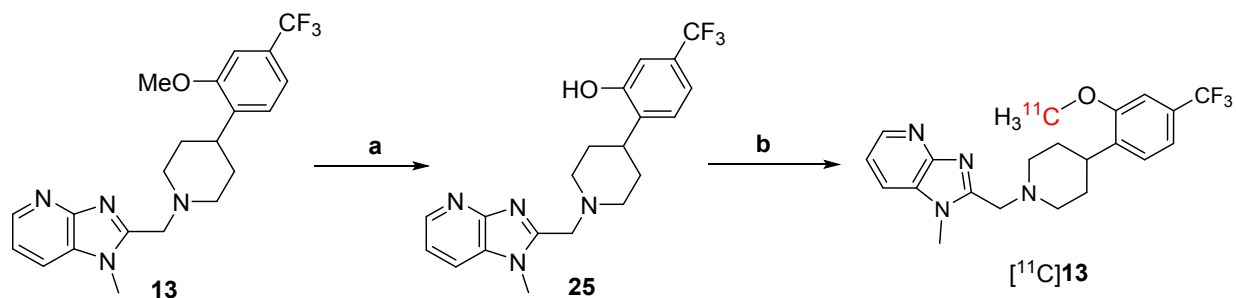


Figure 5. Assessment of BBB permeability for compounds **13-15** via a) PAMPA assay and b) Pgp-Glo™ assay. Pictures were rendered from Prism 5.0.

The Pgp-Glo™ assay was carried out on recombinant human P-gp in a cell membrane fraction to investigate whether the brain penetration will be affected by P-glycoprotein (P-gp) efflux transporter.⁷⁴ The effect of compounds **13-15** on P-gp ATPase activity was examined by comparing the untreated samples and the samples treated with **13-15** to sodium orthovanadate (Na_3VO_4)-treated control. The difference in luminescent signal between Na_3VO_4 -treated samples and samples treated with the test compounds implied P-gp ATPase activity in the presence of the test compound. Verapamil, a P-gp substrate, was used as a positive control in the assay. By comparing basal and verapamil activities to that of **13-15**, it is clearly indicated that **13** is not a P-gp substrate and **15** is a potential P-gp substrate, while **14** displays a moderate P-gp ATPase activity (Figure 5b).

The *in vitro* pharmacological and physicochemical studies reveal that compound **13** has many CNS drug-like properties, including the potent mGluR2 PAM activity and good selectivity against other mGluRs, suitable lipophilicity and PPB, adequate metabolic stability, favorable passive permeability as measured by PAMPA, and no P-gp liability. Based on these results, compound **13** was selected for the radiolabeling and for *in vivo* evaluation as potential mGluR2 PET radioligand.

Radiochemistry. The radiosynthesis of [^{11}C]**13** was achieved via the one-step *O*-methylation of its phenol precursor **23**. Compound **23** was synthesized by demethylation of **13** using boron tribromide (Scheme 2). The radiosynthesis of [^{11}C]**13** was performed by the reaction of **23** (0.5 ± 0.1 mg) with [^{11}C]CH $_3$ I in the presence of aqueous NaOH (5N, 3 μL) in dry DMF (250 μL). The reaction was carried out at 80 $^\circ\text{C}$ for 2 min, followed by purification using a semi-preparative HPLC (Figure S9). The identity of [^{11}C]**13** was confirmed by co-injection with the unlabeled **13** on an analytical HPLC (Figure S10). The radiochemical yield was $20 \pm 2\%$ decay-corrected ($n = 10$), calculated from starting [^{11}C]CO $_2$. The [^{11}C]**13** was then formulated into 10% ethanolic saline solution (pH = 5-6) before injection. The radiochemical and chemical purity were greater than 98%, and the molar activity was 98 ± 30 GBq/ μmol at the end of synthesis (EOS). The overall synthesis time was ca. 50 min, and no radiolysis was observed up to 90 min.



Scheme 2. Synthesis of [^{11}C]**13**. Reagents and conditions: (a) BBr $_3$, DCM, 0 $^\circ\text{C}$ then rt, 2 h. (b) [^{11}C]CH $_3$ I, 5N NaOH, DMF, rt, then 80 $^\circ\text{C}$, 2 min.

1
2
3
4
5 ***Ex vivo* biodistribution studies.** The *ex vivo* whole body biodistribution of [¹¹C]**13** was performed
6
7 in 16 normal male Sprague Dawley rats after intravenous injection of [¹¹C]**13** at several time points
8
9 (5, 20, 30 and 40 min). The uptake value is expressed in the unit of % ID/g. These studies support
10
11 reversible accumulation of [¹¹C]**13**. The highest accumulation of [¹¹C]**13** occurred 5 min after
12
13 administration of radioactivity in the investigated tissue areas but the lungs, where the maximum
14
15 accumulation was at 20 min, and the muscle where the radioactivity steadily increased up to 40
16
17 min (Figure 6). The highest accumulation was measured in the liver ($2.73 \pm 0.02\%$ ID/g) followed
18
19 by kidney ($1.05 \pm 0.07\%$ ID/g), spleen ($0.67 \pm 0.05\%$ ID/g), lung ($0.59 \pm 0.04\%$ ID/g), and heart
20
21 ($0.58 \pm 0.05\%$ ID/g). The high radioactivity uptake in liver and kidney suggest that hepatobiliary
22
23 elimination and renal excretion contribute to the whole body distribution of [¹¹C]**13**. The average
24
25 accumulation of [¹¹C]**13** in the rat brain at 5 min was $0.49 \pm 0.07\%$ ID/g. This result indicates a
26
27 rapid BBB penetration of [¹¹C]**13**, which was consistent with the following *in vivo* brain imaging
28
29 studies.
30
31
32
33
34
35
36
37
38
39
40
41
42
43
44
45
46
47
48
49
50
51
52
53
54
55
56
57
58
59
60

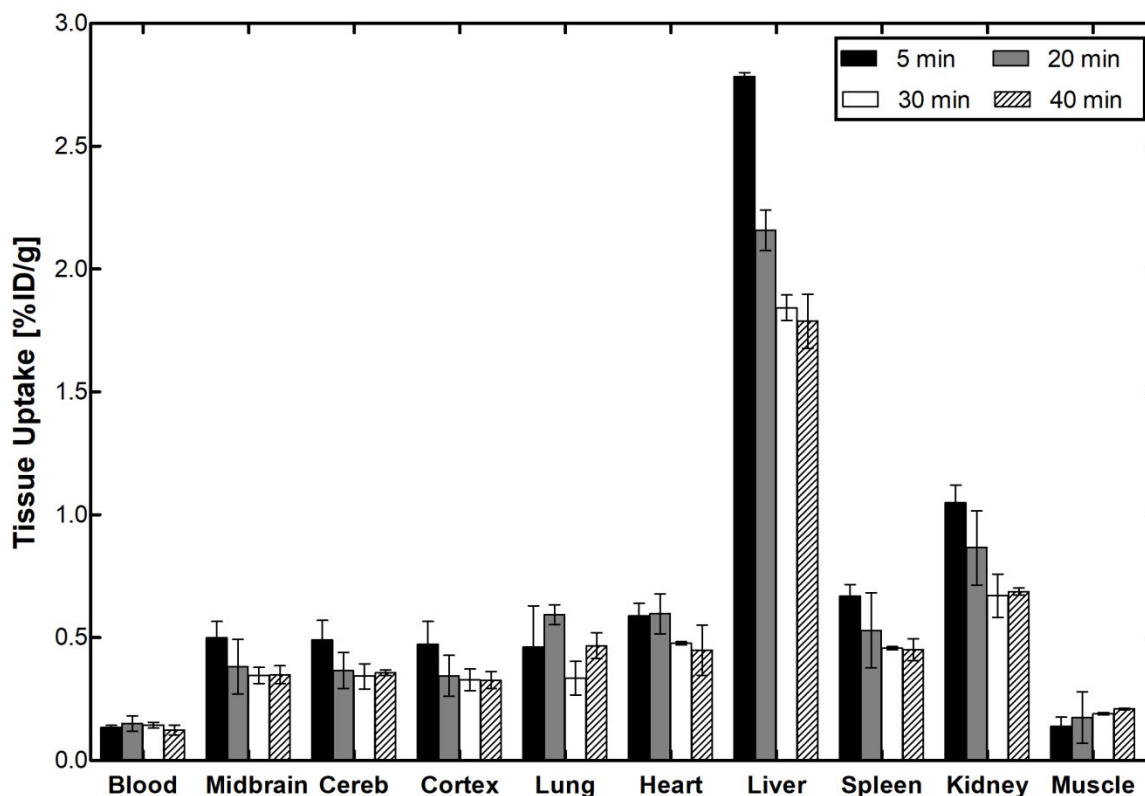
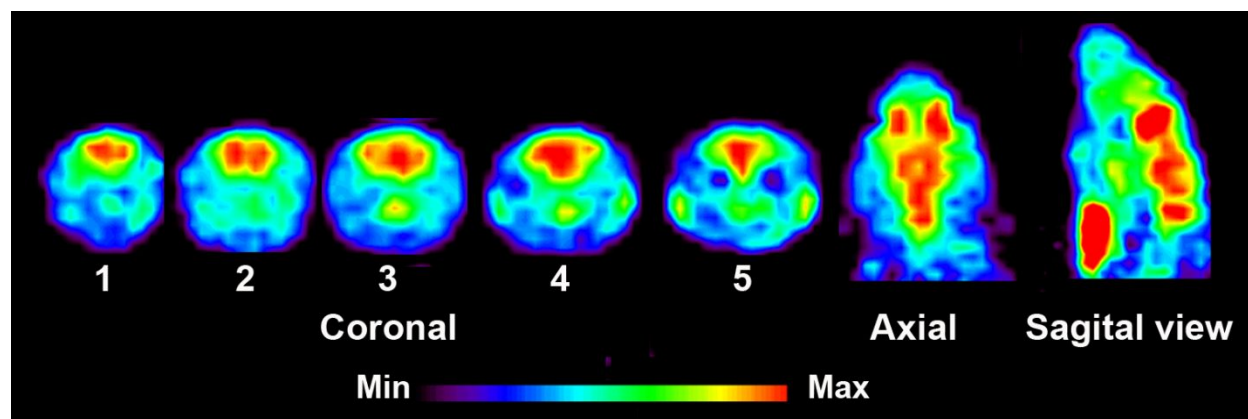


Figure 6. The *ex vivo* biodistribution in rat at four different time points post-[¹¹C]**13** injection.

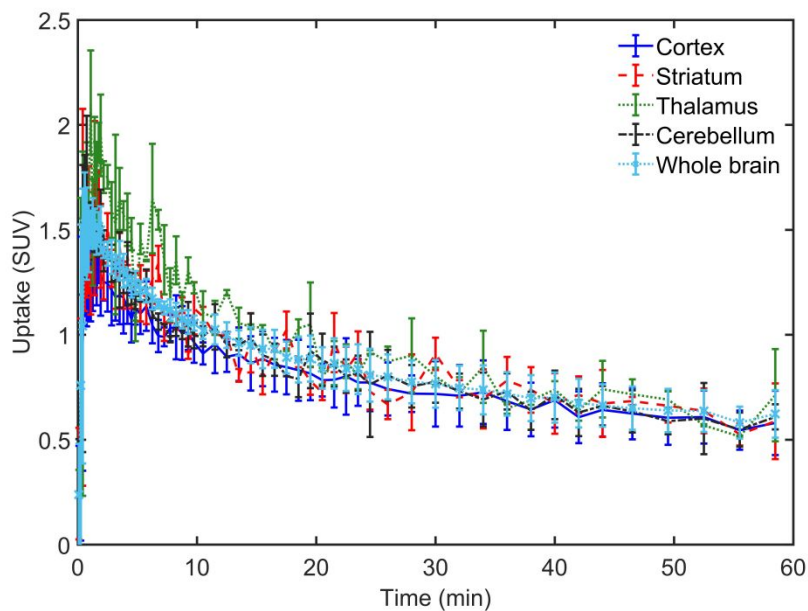
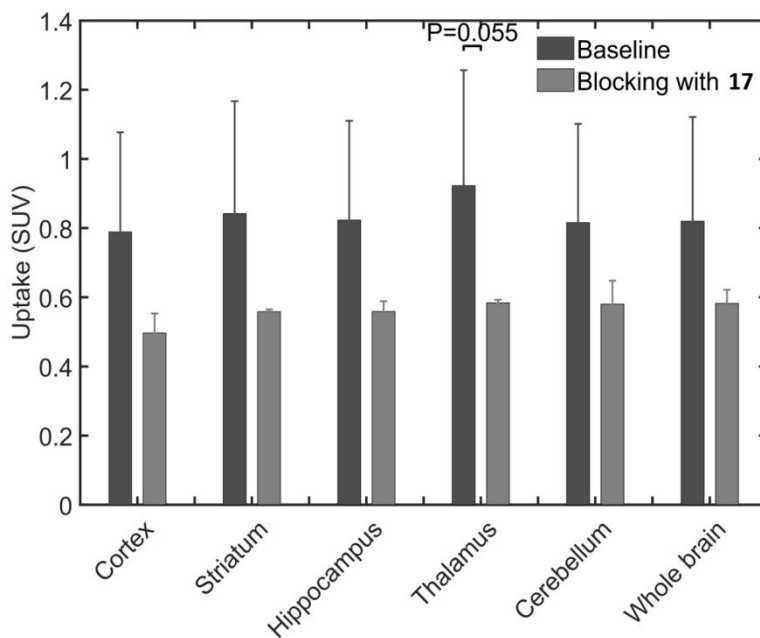
Picture was rendered from Prism 5.0.

PET imaging. *In vivo* characterization of [¹¹C]**13** was conducted with PET imaging using rat (male Sprague-Dawley) models. Dynamic PET scans were performed for 60 min after tail vein injection of [¹¹C]**13**. Representative PET images of cumulative volumetric distribution of [¹¹C]**13** at time interval of 10-15 min are shown on five coronal, axial and sagittal levels (Figure 7). The accumulation of [¹¹C]**13** clearly delineates the mGluR2-rich regions in the rat brain. Time-activity curves (TACs) showed fast radioactivity uptake ($SUV_{max} = 1.8 \pm 0.2$, $n = 9$) and time-dependent accumulation of radioactivity in different brain regions. The highest accumulation of [¹¹C]**13** was in the thalamus, followed by striatum, cerebellum, and cortex. (Figure 8a). Blocking studies were conducted to investigate mGluR2-selective binding of [¹¹C]**13**. Pretreatment with the structurally

1
2
3 distinct *in vivo* active mGluR2 PAM ligand **17** (4 mg/kg i.v.) 10 min before [^{11}C]**13** injection
4
5 resulted in a 28-37% decrease of [^{11}C]**13** uptake in different brain areas at the 10-30 min time
6
7 window (Figure 8b). Statistical analysis showed highly significant ($p < 0.0007$) blocking effect
8
9 concerning combined brain areas while only the thalamus reached local significance. These results
10
11 confirm that [^{11}C]**13** has *in vivo* mGluR2-selective binding in the rat brain.
12
13
14
15
16
17
18
19
20
21
22
23
24
25
26
27
28
29
30



31 **Figure 7.** PET images of [^{11}C]**13** uptake in the rat brain at the time interval 10-15 min. Coronal
32
33 level 1 shows uptake in the cingulate and motor cortex; level 2 in the striatum, level 3 in the
34
35 thalamus and striatum, level 4 in the thalamus and hippocampus and level 5 in the cerebellum.
36
37 Axial and sagittal views show activity distribution in the midbrain level. Slice thickness is 1.25
38
39 mm.
40
41
42
43
44
45
46
47
48
49
50
51
52
53
54
55
56
57
58
59
60

(a)**(b)**

1
2
3 **Figure 8.** *In vivo* binding profile of [¹¹C]**13** in the rat brain. **a)** Time–activity distribution of
4 [¹¹C]**13** in different brain areas show fast accumulation and reversible binding. The data is
5 averaged of six normal Sprague Dawley rats. **b)** The blocking effect was calculated in the time
6 interval 10-30 min after administration of [¹¹C]**13**. Pictures were rendered from Prism 5.0.
7
8
9
10
11
12
13
14
15
16

17 CONCLUSIONS

18
19 We have synthesized and characterized three benzimidazole derivatives (**13-15**) as mGluR2
20 PAMs. Compound **13** demonstrated nanomolar functional activity toward mGluR2 and excellent
21 selectivity over other mGluRs. Further *in vitro* pharmacological and brain permeability evaluations
22 confirmed the potential of compound **13** as PET imaging ligand. A robust and reliable one-step
23 radiosynthetic procedure was established for radiolabeling compound **13** with carbon-11. The
24 desired product [¹¹C]**13** was obtained with a radiochemical yield of 20 ± 2 % (n = 10, decay-
25 corrected) based on [¹¹C]CO₂ and a molar activity of 98 ± 30 GBq/μmol at the end of synthesis
26 (50 min). The *ex vivo* pharmacokinetic results of [¹¹C]**13** suggested its reversible accumulation in
27 most tissue areas and hepatobiliary & urinary excretions. PET imaging studies indicated that
28 [¹¹C]**13** crossed the BBB rapidly and was mainly accumulated in the mGluR2-rich regions of the
29 rat brain such as the thalamus, cerebellum, striatum and cortex. The blocking studies using
30 mGluR2-selective PAM (**17**) significantly reduced the [¹¹C]**13** uptake in these brain regions,
31 indicating the highly selective uptake of [¹¹C]**13** in rat brain. Altogether, these results suggest that
32 compound **13** will be a potential PET imaging ligand for mGluR2 in the brain. Further
33 characterization of the compound **13** is ongoing with an aim for translational PET imaging studies.”
34
35
36
37
38
39
40
41
42
43
44
45
46
47
48
49
50
51
52
53
54
55
56
57
58
59
60

EXPERIMENTAL SECTION

Animal Procedures. The animal studies were approved and done under the guidelines of the Subcommittee on Research Animals of the Massachusetts General Hospital and Harvard Medical School in accordance with the Guide of NIH for the Care and Use of Laboratory Animals.

Materials and Methods. All reagents and starting materials were obtained from the commercial sources including Sigma-Aldrich (St. Louis, MO), Thermo Fisher Scientific, Oakwood Products, Inc., Matrix Scientific, Acros Organics and used as received. The reactions were monitored by TLC using a UV lamp monitored at 254 nm. The reactions were also checked by LC–MS using the Agilent 1200 series HPLC system coupled with a multi-wavelength UV detector and a model 6310 ion trap mass spectrometer (Santa Clara, CA) equipped with an Agilent Eclipse C8 analytical column (150 mm × 4.6 mm, 5 μm). Elution was with a 0.1% formic acid solution of water (A) and acetonitrile (B). The silica gel used in flash column chromatography was from Aldrich (Cat. 60737, pore size 60 Å, 230–400 mesh). Flash chromatography was also performed with a CombiFlash Rf Purification System (Teledyne Isco) using a Silica ReadySep Rf column. The products were identified by LC–MS as well as ¹H NMR, ¹³C NMR and ¹⁹F NMR using a Varian 500 MHz spectrometer. All NMR samples were dissolved in chloroform-d (CDCl₃), methanol-d₄ (CD₃OD) or DMSO-d₆ [(CD₃)₂SO] containing tetramethylsilane as a reference standard. Chemical shifts were expressed as ppm and calculated downfield or upfield from the NMR signal of reference standard. *J* was expressed as Hz, and its splitting patterns were reported as s, d, t, q, or m. HRMS was obtained from the High-Resolution Mass Spectrometry Facility at the University California,

Riverside, using electrospray ionization (ESI)/atmospheric pressure chemical ionization (APCI) technique (Agilent Time of Flight (TOF) LC-MS). The purities of all new compounds were > 95% determined by the Agilent 1200 series HPLC system under a wavelength of 254 nm.

Chemistry. **tert-Butyl(1R,5S,6R)-6-((2-methoxy-4-(trifluoromethyl)phenoxy)methyl)-3-azabicyclo [3.1.0] hexane-3-carboxylate (23).** 2-methoxy-4-(trifluoromethyl)phenol (**22**, 0.45 g, 2.3 mmol) and triphenyl phosphine (0.9 g, 3.5 mmol) were added to a solution of (*1R,5S,6R*)-tert-butyl 6-(hydroxymethyl)-3-azabicyclo[3.1.0]hexane-3-carboxylate (**21**, 0.5 g, 2.3 mmol) in THF under nitrogen. Diethyl azodicarboxylate solution (40 wt. % in toluene, 1.5 g, 3.5 mmol) was added and the reaction was stirred for 16 h. The reaction mixture was stripped in *vacuum* to give orange oil. The crude product was purified via flash chromatography to give **23** as a white solid (0.44 g, 1.14 mmol, 48% yield). ¹H NMR (500 MHz, CDCl₃) δ ppm 7.18 (dd, *J* = 1.0, 8.5 Hz, 1H), 7.08 (d, *J* = 1.8 Hz, 1H), 6.89 (d, *J* = 8.4 Hz, 1H), 4.04-4.08 (m, 1H), 3.92 (s, 3H), 3.82-3.92 (m, 1H), 3.58-3.72 (m, 2H), 3.33-3.42 (m, 2H), 1.59 (d, *J* = 2.7 Hz, 2H), 1.45 (s, 9H), 1.18-1.25 (m, 1H). ¹³C NMR (125 MHz, CDCl₃) δ ppm 154.8, 150.8, 149.5, 124.3 (q, *J* = 271.3 Hz), 123.3 (q, *J* = 32.7 Hz), 118.2 (q, *J* = 4.2 Hz), 112.7, 108.5 (q, *J* = 3.6 Hz), 79.4, 70.7, 56.1, 28.5, 21.4. LC-MS calculated for C₁₉H₂₄F₃NO₄: 387.17; observed: *m/z* 410.0 [M+Na]⁺.

(1R,5S,6R)-6-((2-methoxy-4-(trifluoromethyl)phenoxy)methyl)-3-azabicyclo[3.1.0]

hexane (24). Trifluoroacetic acid (1 mL) was added to a solution of **23** (0.44 g, 1.14 mmol) in dichloromethane (5 mL). The mixture was stirred at room temperature for 2 h. The solvent was removed under reduced pressure to give **24** as a yellow oil (0.3 g, 1.05 mmol, 92% yield). ¹H NMR (300 MHz, methanol-d₄) δ ppm 7.16-7.24 (m, 2H), 7.05 (d, *J* = 8.3 Hz, 1H), 4.0 (d, *J* = 6.7 Hz, 2H), 3.88 (s, 3H), 3.42-3.53 (m, 4H), 1.94-1.98 (m, 2H), 1.39-1.47 (m, 1H). ¹³C NMR (75 MHz,

1
2
3 methanol-d₄) δ ppm 152.4, 151.1, 125.8 (q, $J = 270.5$ Hz), 124.4 (q, $J = 32.6$ Hz), 119.4 (q, $J = 4.2$
4 Hz), 114.4, 109.7 (q, $J = 3.6$ Hz), 70.7, 56.7, 22.2, 21.0. LC-MS calculated for C₁₄H₁₆F₃NO₂:
5
6 287.11; observed: m/z 288.1 [M+H]⁺.
7
8

9
10 **2-((4-(2-Methoxy-4-(trifluoromethyl)phenyl)piperidin-1-yl)methyl)-1-methyl-1H-**
11 **imidazo[4,5-b]pyridine (13).** Trimethylamine (0.22 g, 2.16 mmol), magnesium sulfate (0.65 g,
12 5.41 mmol) and 1-methyl-1H-imidazo[4,5-b]pyridine-2-carbaldehyde (**19**, 0.81 mmol, 0.16 g)
13 were added to a solution of 4-(2-methoxy-4-(trifluoromethyl)phenyl)piperidine (**18**, 0.54 mmol,
14 0.13 g) in 1,2-dichloroethane (5 mL) under nitrogen. The mixture was stirred at room temperature
15 for 30 min before sodium triacetoxyborohydride (0.17 g, 0.81 mmol) was added. The reaction
16 mixture was then stirred overnight at room temperature and then quenched with dichloromethane.
17 The organic phase was washed with water and brine. The aqueous phase was extracted with
18 dichloromethane. Combined organic layer was dried over sodium sulfate. The solvent was
19 removed at reduced pressure, and the residue was purified by flash column chromatography to
20 give the product as a white solid (0.35 mmol, 0.14 g, 65% yield). ¹H NMR (500 MHz, CD₃OD): δ
21 8.41 (d, $J = 5.0$ Hz, 1H), 8.02 (d, $J = 8.5$ Hz, 1H), 7.34-7.37 (m, 2H), 7.20 (d, $J = 7.5$ Hz, 1H), 7.14
22 (s, 1H), 4.01 (s, 3H), 3.94 (s, 2H), 3.89 (s, 3H), 3.31-3.32 (m, 3H), 2.33-2.37 (m, 2H), 1.72-1.83
23 (m, 4H). LC-MS calculated for C₂₁H₂₃F₃N₄O: 404.18; observed: m/z 405.15 [M+H]⁺.
24
25
26
27
28
29
30
31
32
33
34
35
36
37
38
39
40
41

42 **2-((4-(2-Methoxy-4-(trifluoromethyl)phenyl)piperidin-1-yl)methyl)-5,6-dihydro-4H-**
43 **imidazo [4,5,1-ij][1,7]naphthyridine (14).** In a similar procedure as described for synthesizing
44 **13**, compound **14** was prepared by using **18** (100 mg, 0.34 mmol) and 5,6-Dihydro-4H-
45 imidazo[4,5,1-ij][1,7]naphthyridine-2-carbaldehyde (**20**, 110 mg, 0.51 mmol) to give the product
46 as a white solid (76 mg, 0.18 mmol, 52% yield). ¹H NMR (500 MHz, (CD₃)₂SO): δ 8.50 (d, $J =$
47 5.0 Hz, 1H), 7.40 (d, $J = 8.5$ Hz, 1H), 7.25 (d, $J = 8.5$ Hz, 1H), 7.20 (s, 1H), 7.01 (d, $J = 4.5$ Hz,
48 5.0 Hz, 1H), 7.40 (d, $J = 8.5$ Hz, 1H), 7.25 (d, $J = 8.5$ Hz, 1H), 7.20 (s, 1H), 7.01 (d, $J = 4.5$ Hz,
49
50
51
52
53
54
55
56
57
58
59
60

1
2
3 1H), 4.33 (t, $J = 6.0$ Hz, 2H), 4.02 (s, 1H), 3.29 (s, 1H), 3.86 (s, 3H), 2.93-2.97 (m, 5H), 2.15-2.48
4 (m, 5H), 1.60-1.71 (m, 4H). LC-MS calculated for $C_{23}H_{25}F_3N_4O$: 430.20; observed: m/z 431.20
5
6
7
8 [M+H]⁺.

9
10 **2-(((1R,5S,6R)-6-((2-methoxy-4-(trifluoromethyl)phenoxy)methyl)-3-azabicyclo[3.1.0]**
11 **hexan-3-yl)methyl)-1-methyl-1H-imidazo[4,5-b]pyridine (15).** In a similar procedure as
12 described for synthesizing **13**, compound **15** was prepared by using **19** (HCl salt, 50 mg, 0.25
13 mmol) and **24** (HCl salt, 98 mg, 0.304 mmol) to give product as a white solid (31 mg, 0.072 mmol,
14 28% yield). ¹H NMR (500 MHz, CDCl₃): δ 8.47 (d, $J = 4.5$ Hz, 1H), 7.59 (d, $J = 7.5$ Hz, 1H), 7.29
15 (m, 2H), 7.02 (s, 1H), 6.83 (d, $J = 8.5$ Hz, 1H), 3.93 (s, 2H), 3.85 (s, 3H), 3.83 (d, $J = 7.5$ Hz, 2H),
16 3.78 (s, 3H), 2.96 (d, $J = 9.0$ Hz, 2H), 2.57 (d, $J = 8.0$ Hz, 2H), 1.67(m, 1H), 1.50 (s, 2H). ¹³C
17 NMR (125 MHz, CDCl₃): δ 155.0, 154.4, 151.0, 149.3, 144.5, 128.4, 123.1, 122.8, 118.2, 117.6,
18 116.9, 112.4, 108.4, 71.3, 56.0, 54.5, 51.5, 30.1, 21.5, 18.6. ¹⁹F NMR (470 MHz, CDCl₃): δ -57.6.
19
20
21
22
23
24
25
26
27
28
29
30
31
32
33
34
35
36
37
38
39
40
41
42
43
44
45
46
47
48
49
50
51
52
53
54
55
56
57
58
59
60
LC-MS calculated for $C_{22}H_{23}F_3N_4O_2$: 432.18; observed: m/z 433.15 [M+H]⁺. HRMS m/z
calculated for $C_{22}H_{24}F_3N_4O_2$ [M+H]⁺, 433.1851, found m/z 433.1863.

35
36 **3-(Cyclopropylmethyl)-7-((4-(2,4-difluorophenyl)piperazin-1-yl)methyl)-8-**
37 **(trifluoromethyl)[1,2,4]triazolo[4,3-a]pyridine (17, JNJ-46356479).** In a similar procedure as
38 described for synthesizing **13**, compound **17** was prepared by using 3-(cyclopropylmethyl)-8-
39 (trifluoromethyl)-[1,2,4]triazolo[4,3-a]pyridine-7-carbaldehyde (50 mg, 0.19 mmol) and 1-(2,4-
40 difluorophenyl)piperazine (41.6 mg, 0.21 mmol), TEA (0.11 mL, 0.76 mmol), MgSO₄ (0.229 g,
41 1.9 mmol) and NaBH(OAc)₃ (60.4 mg, 0.285 mmol) in DCM (3 mL) to give product as a pale-
42 yellow solid (44.2 mg, 0.098 mmol, 51.6% yield). ¹H NMR (500 MHz, CDCl₃) δ 8.23 (d, $J = 7.5$
43 Hz, 1H), 7.45 (d, $J = 6.5$ Hz, 1H), 6.90-6.91 (m, 1H), 6.78-6.81 (m, 2H), 3.81 (s, 2H), 3.10 (d, J
44
45
46
47
48
49
50
51
52
53
54
55
56
57
58
59
60

= 6.5 Hz, 2H), 3.01-3.09 (m, 4H), 2.63-2.75 (m, 4H), 1.21-1.26 (m, 1H), 0.60-0.62 (m, 2H), 0.33-0.34 (m, 2H). LC-MS calculated for C₂₂H₂₂F₅N₅: 451.18; observed: *m/z* 452.05 [M+H]⁺.

2-((1-(1-Methyl-1H-imidazo[4,5-b]pyridin-2-yl)methyl)piperidin-4-yl)-5-(trifluoromethyl)phenol (25). The boron tribromide solution (1 mL, 1 M in DCM, 1 mmol) was added dropwise to a solution of compound **13** (70 mg, 0.173 mmol) in 3 mL dichloromethane at 0 °C. The mixture was slowly warmed to room temperature and stirred for another 2 h. After the reaction was completed, 5 mL of saturated sodium bicarbonate was added, and the mixture was extracted with dichloromethane. The crude product was purified by flash column chromatography to give product as a white solid (60 mg, 0.153 mmol, 88% yield). ¹H NMR (500 MHz, CD₃OD): δ 8.42 (d, *J* = 5.0 Hz, 1H), 8.03 (d, *J* = 8.5 Hz, 1H), 7.34-7.37 (m, 1H), 7.28 (d, *J* = 7.5 Hz, 1H), 7.05 (d, 1H, *J* = 7.5 Hz), 7.00 (s, 1H), 4.01 (m, 3H), 3.94, (m, 2H), 2.99-3.06 (m, 3H), 2.34-2.38 (m, 2H), 1.73-1.86 (m, 4H). ¹³C NMR (125 MHz, CD₃OD): δ 155.4, 155.0, 153.7, 143.6, 136.6, 128.7, 126.8, 125.4, 123.3, 118.7, 118.0, 115.3, 115.3, 111.0, 54.6, 54.2, 35.1, 31.3, 29.5. LC-MS calculated for C₂₀H₂₁F₃N₄O: 390.17; observed: *m/z* 391.10 [M+H]⁺. HRMS *m/z* calculated for C₂₀H₂₂F₃N₄O [M+H]⁺, 391.1746, found *m/z* 391.1765.

Radiochemistry. ¹¹CO₂ was obtained via the ¹⁴N(p,α)¹¹C reaction on nitrogen with 2.5% oxygen, 16 MeV protons (GE Healthcare, PETtrace), and trapped on molecular sieves in a TRACERlab FX-MeI synthesizer (GE Healthcare). ¹¹CH₄ was obtained by the reduction of ¹¹CO₂ in the presence of hydrogen at 350 °C and passed through an oven containing I₂ to produce ¹¹CH₃I via a radical reaction. ¹¹CH₃I was trapped in a 5 mL V-vial containing a solution of excess **25** (0.5 ± 0.2 mg) and an aqueous 5N NaOH (3 uL) in dry dimethylformamide (250 μL) at room temperature and then heated at 80 °C for 2 min. The reaction mixture was diluted with 1.0 mL of water and purified using a HPLC system equipped with a semi-preparative column (Waters XBridge, C18, 250 × 10

1
2
3 mm, 5 μ), a UV detector monitored at 254 nm, and a radioactivity detector. The product was eluted
4
5 with acetonitrile/water/TFA (30/70/0.7) at a flow rate of 5 mL/min. The fractions corresponding
6
7 to [^{11}C]**13** ($t_{\text{R}} = 11$ min) were collected into a large dilution vessel, which was pre-loaded with 2
8
9 mL of 8.4% sodium bicarbonate for injection, USP (Hospira) and 23 mL of sterile water for
10
11 injection, USP. The product was loaded onto a C18 light cartridge, (Waters; pre-activated with 4
12
13 mL of EtOH followed by 10 mL of SWFI). The C18 light cartridge was washed with 10 mL of
14
15 SWFI to remove traces of salts, residual acetonitrile and TFA. The C18 light cartridge was then
16
17 eluted with 1 mL of dehydrated ethyl alcohol (USP) and followed by 10 mL of 0.9% sodium
18
19 chloride solution (USP) into a product collection vessel. The formulated solution was filtered
20
21 through a vented Millipore-GV 0.22 μ sterilizing filter (EMD Millipore) into a 10 mL vented sterile
22
23 vial.
24
25
26
27

28
29 Radiochemical purity and chemical quality were measured by an analytical HPLC equipped
30
31 with an analytical column (Waters, XBridge, C18, 3.5 μ , 4.6 \times 150 mm), a UV detector monitored
32
33 at 254 nm, and a radioactivity detector, which was eluted with a solution (acetonitrile/0.1%TFA
34
35 water = 30/70) at a flow rate of 1 mL/min. [^{11}C]**13** was eluted \sim 6 min (chemical and radiochemical
36
37 purities $> 98\%$, $n = 10$). The radiosynthesis time was 50 min from the end of bombardment (EOB).
38
39 The molar activity was 98 ± 30 GBq/ μmol at the end of synthesis (EOS).
40
41

42
43 **Molecular modeling.** The mGluR2 receptor model structure was built in YASARA⁴⁵ using a
44
45 series of structures from the Protein Data Bank (PDB). These structures were obtained after a
46
47 BLAST⁷⁵ search of the mGluR2 sequence against the PDB. The model was built by manually
48
49 selecting from these template structures with sequence homology to mGluR2. These templates are
50
51 mGluR1 complexed with glutamate (PDB ID:1EWK)⁴⁶, mGluR5 complexed with glutamate (PDB
52
53 ID: 3LMK)⁴⁷ and Metabotropic Glutamate Receptor 5 Apo Form (PDB ID 6N52)⁴⁸. Using these
54
55
56
57
58
59
60

1
2
3 three structures as templates, a hybrid model for mGluR2 was built in YASARA. Results of model
4
5 evaluations are given in the Supporting Information.
6

7
8 To prepare the ligands for docking, the ligands were drawn on ChemDraw Professional 16.0
9
10 by PerkinElmer and were converted into PDB format in Avogadro 1.2⁷⁶. These ligands were
11
12 further optimized in Avogadro before docking. Docking was performed into the model structure
13
14 with AutoDock⁵⁶ embedded in YASARA⁴⁵.
15

16
17 **GloSensor cAMP functional assay.** HEK-293 cells were maintained with complete Dulbecco's
18
19 modified Eagle's medium (DMEM), which was composed of 10% fetal bovine serum (FBS), 2
20
21 mM L-glutamine, 100 units/mL penicillin G, 100 µg/mL streptomycin at 37 °C in the presence of
22
23 5% CO₂. HEK-293 stable cell lines with tetracycline inducible expression of mGluR1, mGluR2,
24
25 mGluR4, mGluR6 or mGluR8 were maintained with complete DMEM with Hygromycin B (100
26
27 µg/mL), Blasticidin (15 µg/mL) at 37°C in the presence of 5% CO₂.
28
29

30
31 The Gq coupled receptors (mGluR1 and mGluR5) were tested using Ca²⁺ mobilization assay.
32
33 mGluR1 stable cell lines were plated into poly-L-lysine (PLL) coated 384-well black clear bottom
34
35 cell culture plates with complete Basal Medium Eagle (BME) buffer, which was composed of 10%
36
37 dialyzed FBS, penicillin G (100 units/mL), streptomycin (100 µg/mL) with Tetracycline (1 µg/mL)
38
39 at density of 20,000 cells in 40 µl per well for overnight. On the other hand, HEK-293 Cells
40
41 transiently transfected using the calcium phosphate method with cDNA encoding mGluR5 for 40
42
43 h were plated into the plate with complete BME at density of 20,000 cells in 40 µL per well for 8
44
45 h. mGluR1 stable cells or cells transiently expressing mGluR5 were incubated with 20 µL of the
46
47 calcium dye (FLIPR Calcium 4 Assay Kit; Molecular Devices) diluted in the assay buffer (1×
48
49 HBSS, 2.5 mM probenecid, and 20 mM HEPES, pH 7.4) for 45 min at 37 °C and 15 min at room
50
51
52
53
54
55
56
57
58
59
60 temperature. To measure agonist activity of receptors, the drug plates were prepared with different

1
2
3 concentrations of test or reference compound at 3 times the desired final concentration. When
4 measuring antagonist activity, another drug plate which contained EC₈₀ concentration of the
5 reference drug was prepared. Once loaded in FLIPR (Molecular Devices), basal fluorescence was
6 measured for 10 s, then 10 µL of test or reference compounds were added, followed by continued
7 fluorescence measurement for an additional 120 s. Raw data were plotted as a function of molar
8 concentration of the compound with Prism 5.0 (GraphPad Software).
9

10
11
12
13
14
15
16
17 The Gi/o coupled receptors (mGluR2, mGluR3, mGluR4, mGluR6 and mGluR8) were tested
18 using cAMP assay. Promega's split luciferase based GloSensor cAMP biosensor technology was
19 used in determining Gi-GPCR mediated cAMP production in live cells. On the cells stably
20 expressing mGluR2, mGluR3, mGluR4, mGluR6 or mGluR8, GloSensor cAMP DNA construct
21 was transfected overnight. Cells were seeded into PLL coated 384-well white clear bottom cell
22 culture plates with complete BME Buffer with Tetracycline (1 µg/mL) at a density of 20,000 cells
23 for another 24 h. The cell medium was removed and then 20 µl of buffer was loaded. To measure
24 the agonist activity, 10 µL of 3x test compound solution was added 15 min before addition of 10
25 µl of luciferin/isoproterenol mixture at a final concentration of 4 mM and 200 nM, respectively,
26 followed by counting of the plate. To measure the PAM or antagonist activity, cells were pre-
27 incubated with test compound for 15 min before addition of EC₂₀ or EC₈₀ concentration of a
28 reference agonist for another 15 min. Then 10 µl of luciferin/isoproterenol mixture at a final
29 concentration of 4 mM and 200 nM, respectively, was added for 15 min followed by counting of
30 the plate. In these experiments, isoproterenol was used to activate endogenous β₂ adrenergic
31 receptors expressed in HEK293 T cells to activate the endogenous G_s protein. Luminescence was
32 counted in a TriLux luminescence counter. Data were analyzed with Prism 5.0 (GraphPad
33 software).
34
35
36
37
38
39
40
41
42
43
44
45
46
47
48
49
50
51
52
53
54
55
56
57
58
59
60

1
2
3 Compounds were tested for their potency in dose-response experiments. Eight-point dose
4 response curves were performed in duplicate twice on two separate lots of cells (sometimes a third
5 curve might be needed if in the first experiment the range of concentrations used was outside of
6 the active range). For antagonists, these curves were performed in the presence of the EC₈₀
7 concentration of the agonist. For each compound, the results from four replicates were averaged
8 and then either EC₅₀ or IC₅₀ values were calculated by non-linear regression using the 4-parameter
9 logistic equation. Results were reported as EC₅₀ or IC₅₀ values for each tested compound (and
10 receptor) and include the EC₅₀ or IC₅₀ values of a known agonist or antagonist for comparison
11 purposes.
12
13
14
15
16
17
18
19
20
21
22
23
24
25

26 ***In vitro* characterization.** The Log P was determined using a reversed-phase HPLC method.
27 First, seven reference compounds were examined to obtain the linear regression of the log P against
28 the log of capacity factors by the expression: $\log P_{ow} = a + b * \log k$. The Log P of these reference
29 compounds was already been determined. The capacity factor k was calculated by the expression:
30 $k = (t_R - t_0)/t_0$. The retention time t_R of test compound was determined on the HPLC (Agilent 1260
31 infinity II LC System, XTerra™ MS C18 5 μ 2.1 \times 250 mm, methanol/water=75/25, 0.25 mL/min).
32 The dead-time t_0 was measured by using thiourea. All measurements were done with triplicate
33 three parallels and results are given in Table S4. The linear regression equation of the Log P against
34 the log of capacity factors was generated in Excel: $\log P_{ow} = 3.049 + 2.429 * \log k$, where R² was
35 0.9964 (Figure S9). The retention time of compound **13-15** was also determined on the HPLC
36 under the same condition and each test was repeated three times (Table S5).
37
38
39
40
41
42
43
44
45
46
47
48
49
50
51

52 In the plasma protein binding assay, disposable RED device inserts (product 90006) were from
53 Thermo Scientific (Waltham, MA). Each insert was made of two side-by-side chambers separated
54
55
56
57
58
59
60

1
2
3 by a vertical cylinder of dialysis membrane (MWCO ~8,000) validated for minimal non-specific
4 binding. A stock solution of the test compound in DMSO was spiked into the rat plasma to reach
5 a concentration of 10 μ M. 400 μ L of sample solution was placed into the sample chamber of the
6 RED device, and 600 μ L of phosphate-buffered saline (PBS) was added to the buffer chamber of
7 the RED device. Samples were prepared in triplicates. The plate was covered with aluminum
8 sealing cover and incubated at 37 $^{\circ}$ C on an orbital shaker at approximately 200 rpm for 5 h. After
9 incubation, 300 μ L of post-dialysis samples from the buffer and sample chambers were transferred
10 to different microcentrifuge tubes. To the buffer sample was added 300 μ L of plasma, and an equal
11 volume of buffer was added to the collected plasma sample. 600 μ L of cold acetonitrile was added
12 to the samples, and the samples were vortexed and incubated for 30 min on ice and then were
13 centrifuged at 14000 rpm for 10 min. Supernatant was transferred to vial for HPLC analysis
14 (XTerraTM MS C18 5 μ , 2.1 \times 250 mm column; Gradient elution from 5% to 90% B in 30 min;
15 0.1 M ammonium formate in water (A) and acetonitrile (B); UV 254 nm; 100 μ L of injection
16 volume). The percentage of the test bound compound was calculated as % Free = (Concentration
17 in buffer chamber/Concentration in plasma chamber) \times 100%; % Bound = 100% - % Free (Table
18 S6).

19
20
21
22
23
24
25
26
27
28
29
30
31
32
33
34
35
36
37
38
39
40
41 Compound stability in rat serum was examined using a published method.⁶⁸ Rat serum (100
42 μ L, Abcam, Inc, No. ab7488) and test compound or control compound (2.5 μ L, 1 mM in DMSO)
43 was added to the individual tube. The tube was vortexed and incubated at 37 $^{\circ}$ C. During the
44 incubation, aliquots of 50 μ L samples were quenched with ice-cold acetonitrile at 0, 15, 30, 60,
45 and 120 min time points, respectively. After mixing, the quenched samples were centrifuged, and
46 the supernatant was withdrawn for analysis by HPLC (Agilent 1260 infinity II LC System,
47 XTerraTM MS C18, 5 μ , 2.1 \times 250 mm, 20 mM ammonium formate (A)/acetonitrile (B), 0.25
48
49
50
51
52
53
54
55
56
57
58
59
60

1
2
3 mL/min, gradient of 5% to 100% B). The samples were assayed at least three times. Compound
4
5 **25** was used as internal standard while diltiazem was used as a positive control. The percentage
6
7 remaining was calculated by (peak area at the specific time point)/(peak area at 0 min) × 100%
8
9 (Table S7).
10

11
12 Compound stability in rat liver microsomal was tested using a published method.^{68,69} In a vial
13
14 1.5 μL of test compound (1 mM in DMSO stock solution) was mixed with 432 μL of PBS (50
15
16 mM, pH 7.4). The mixture was kept at 37 °C for 10 min before adding 13 μL of Sprague–Dawley
17
18 rat liver microsomes (Sigma-Aldrich, No. M9066). The vial was vortexed and shaken at 37 °C for
19
20 5 min, followed by addition of 50 μL of NADPH (10 mM in PBS stock solution) to start the
21
22 reaction. The mixture was incubated at 37 °C for 0, 5, 15, 30, 45 min, respectively, and quenched
23
24 by addition of 250 μL of ice-cold acetonitrile and 3 μL of the internal standard (0.5 mM in DMSO).
25
26 The quenched solutions were centrifuged at 10,000g for 15 min. The supernatant was collected
27
28 and quantitated by RP-HPLC (Phenomenex Luna® column 5 μ C18, 100 Å, 250 x 4.6 mm; 0.7
29
30 mL/min, 15 min, Acetonitrile/water/0.1% FA). The procedure was repeated three times for each
31
32 compound. Compound **25** was used as internal standard and compound ML128 served as positive
33
34 control. The percentage of remaining intact test-compound was calculated by (peak area at the
35
36 specific time point)/(peak area at 0 min)×100%. Each procedure was repeated three times (Tables
37
38 S8 & S9).
39
40
41
42
43

44
45 The solution stability of **13** was examined in the aqueous buffers at different pH values. 50 μL
46
47 of compound in DMSO (0.25 mM) was added to the sodium acetate-KCl-HCl buffer (950 μL, 20
48
49 mM, pH 5.0), phosphate buffer (950 μL, 20 mM, pH 7.4), and boric acid-KCl-NaOH buffer (950
50
51 μL, 20 mM, pH 9.4), respectively. The mixtures were incubated for 2 h at 37 °C and analyzed by
52
53 HPLC (Phenomenex Luna® column, 5 μm C18, 100 Å, 250 x 4.6 mm, eluents: CH₃CN/H₂O in 0.1%
54
55
56
57
58
59
60

1
2
3 formic acid). The area under curve (AUC) values of **13** was monitored at 0, 15, 30, 60, and 120
4
5 min time points (n = 2, Table S10).
6

7
8 In the PAMPA assay, polar brain lipid (PBL) was purchased from Avanti Polar Lipids
9
10 (Alabaster, AL). Theophylline, caffeine, and dodecane were purchased from Sigma-Aldrich. The
11
12 96-well acceptor filter plate (polyvinylidene difluoride membrane, pore size 0.45 μm) and the
13
14 donor microplate were obtained from Merck Millipore Bioscience (Bedford, MA). Test compound
15
16 was dissolved in DMSO at 5 mg/mL, and further diluted in phosphate buffer (pH 7.4) to obtain
17
18 the sample solution at a final concentration of 25 $\mu\text{g/mL}$. The acceptor wells were coated with 4
19
20 μL of porcine polar brain lipid (PBL) in dodecane (20 mg/mL) before 200 μL of phosphate buffer
21
22 was added. To the corresponding donor well, 300 μL of the sample solution (n = 5) was added.
23
24 The acceptor well was carefully put on the donor plate and kept for 18 h. After incubation, the
25
26 acceptor plate was separated from the donor plate and the concentration of the test compounds in
27
28 both acceptor and donor wells was determined using a UV plate reader (SpectraMax M Series
29
30 Multi-Mode Microplate Readers). Verapamil ($P_e = 16 \times 10^{-6}$ cm/s) and theophylline ($P_e = 0.12$
31
32 $\times 10^{-6}$ cm/s) were used as positive and negative control compounds, respectively.
33
34
35
36
37

38 The P-gp ATPase activity was measured with the Pgp-Glo™ assay system with human P-gp
39
40 membrane by following the manufacturer's instructions (Promega, Co. USA). The assay relies on
41
42 the ATP dependence of the light-generating reaction of firefly luciferase. Briefly, 25 μg of P-gp
43
44 membrane was incubated at 37 °C with one of these samples including Na_3VO_4 (100 μM), solvent
45
46 control (0.1% DMSO), quercetin (100 μM), the test compound (200 μM), verapamil (100 μM),
47
48 verapamil (100 μM) plus the test compound (100 μM). The ATPase reaction was initiated by
49
50 addition of MgATP (5 mM) and followed by incubation for 40 min at 37 °C. The reaction was
51
52 stopped, and the remaining unmetabolized ATP was detected as a luciferase-generated
53
54
55
56
57
58
59
60

1
2
3 luminescence signal by addition of ATP detection reagent. Following a room-temperature signal-
4 stabilization period (20 min), luminescence was read on a Veritas microplate luminometer (Tuner
5 Designs, San Francisco, CA). P-gp ATPase activity was presented as a drop-in luminescence of
6 samples compared to that treated with Na_3VO_4 .
7
8
9

10
11
12 **Whole body biodistribution study.** The quantitative biodistribution of [^{11}C]**13** was done using
13 16 healthy Sprague Dawley rats (weight 330-370 g). After anesthetization (2% isoflurane with
14 oxygen flow of 1.5 L/min) the rats were administrated with the [^{11}C]**13** (30-42 MBq (0.81-1.14
15 mCi) using tail vein injection and sacrificed by decapitation at the time points 5, 20, 30 or 40 min
16 after administration of the radioactivity. The tissue samples including blood, midbrain, cerebellum,
17 cortex, lung, heart, liver, spleen, kidney and muscle were rapidly collected into pre-weighted
18 gamma-counting tubes and measured with standards (samples of [^{11}C]**13**) using PerkinElmer
19 Wizard2 2480 gamma-counter. Tubes were weighted, and the net mass of the tissue samples was
20 determined and the percent of the injected radioactivity (% ID/g) in the samples was calculated.
21
22
23
24
25
26
27
28
29
30
31
32

33 ***In vivo* characterization.** Altogether nine normal Sprague Dawley rats (male, 275-500 g) were
34 used in thirteen studies to investigate *in vivo* imaging characteristics of [^{11}C]**13**. Four rats had
35 control studies followed by the “blocking” studies and 5 rats had only control studies to investigate
36 binding characteristics of [^{11}C]**13**. For the imaging studies rats were anesthetized with
37 isoflurane/nitrous oxide (1.0-1.5% isoflurane, with oxygen flow of 1-1.5 L/min) and the tail vein
38 was catheterized for administration of the imaging ligand ([^{11}C]**13**). The rats were adjusted into
39 the scanner for imaging position (Triumph II Preclinical Imaging System, Trifoil Imaging, LLC,
40 Northridge, CA). The vital signs such as heart rate and/or breathing were monitored throughout
41 the imaging. Data acquisition of 60 min was started from the injection of radioligand [^{11}C]**13** (20-
42 41 MBq (0.54-1.11 mCi) i.v.).
43
44
45
46
47
48
49
50
51
52
53
54
55
56
57
58
59
60

1
2
3 The “cold” compound **17** was used to investigate selectivity and sensitivity of [¹¹C]**13** for the
4 mGluR2. For injection **17** was dissolved into saline with 20% HP-B-CD with pH under 5.5. The
5
6
7 “cold” compounds were administered (i.v., 4 mg/kg) 10 min before the radioactivity.
8
9

10 CT scan was performed after every PET imaging study to obtain anatomical information and
11 correction for attenuation. The PET imaging data were corrected for uniformity, scatter, and
12 attenuation and processed by using maximum-likelihood expectation-maximization (MLEM)
13 algorithm with 30 iterations to dynamic volumetric images (18×10”, 14×30”, 20×60”, 10×180”).
14
15 CT data were reconstructed by the modified Feldkamp algorithm using matrix volumes of
16 512×512×512 and pixel size of 170 μm. The ROIs, i.e., whole brain, thalamus, hippocampus,
17 cortex, striatum, and cerebellum, were drawn onto coronal PET slices according to the brain
18 outlines as derived from the rat brain atlas and corresponding TACs (time-activity curves) were
19 created by PMOD 3.2 (PMOD Technologies Ltd., Zurich, Switzerland). Percent changes between
20 the control and blocking studies were calculated in the selected brain areas at the 10-30 min time
21 window after injection of [¹¹C]**13**. Statistical significance between the baseline and blocking
22 studies were calculated using the two-sample t-test.
23
24
25
26
27
28
29
30
31
32
33
34
35
36
37
38
39

40 **ASSOCIATED CONTENT**

41 **Supporting Information**

42 The Supporting Information is available free of charge on the ACS Publications website at DOI:

43 Molecular formular strings (CSV)

44 Preparation and structural evaluation of mGluR2 homology model, prediction of mGluR2 binding
45 site, *in vitro* mGluR2 binding assay, mGluR2 functional assay, ligand lipophilicity assay, plasma
46 protein binding assay, evaluation of compounds’ plasma stability, microsome stability and solution
47
48
49
50
51
52
53
54
55
56
57
58
59
60

1
2
3 stability, purification and characterization of [¹¹C]**13**, and HPLC spectra for compounds **13-15**
4
5 (PDF)
6

7 The PDB coordinates of the mGluR2 homology model (PDB)
8
9

14 15 **AUTHOR INFORMATION**

16 17 **Corresponding Authors**

18
19 *G.Y.; <https://orcid.org/0000-0003-4817-0052>; Phone: 857-210-6386; Email:

20
21 gyyuan@mgh.harvard.edu
22

23
24 *ZZ.; Phone: 617-643-4887; Email: zzhang@nmr.mgh.harvard.edu
25

26
27 *A-L.B.; <https://orcid.org/0000-0002-3814-868X>; Phone: 617-726-3709; Email:

28
29 abrownell@mgh.harvard.edu
30
31
32

33 34 **Author Contributions**

35 #G.Y. and X.Q. contributed equally. The manuscript was written through contributions of all
36
37 authors.
38

39 40 **Notes**

41
42 The authors declare no conflict interest.
43
44
45

46 47 **ACKNOWLEDGEMENTS**

48
49 This project was financially supported by NIH grants [1R01EB021708 and 1R01NS100164] and
50
51 the grants 1S10RR023452-01 and 1S10OD025234-01 for the imaging instrumentation and
52
53 characterization of the organic compounds. mGluR1-6 and mGluR8 agonist and antagonist
54
55
56
57
58
59
60

1
2
3 functional data as well as mGluR2 PAM activity were generously provided by the National
4
5 Institute of Mental Health's Psychoactive Drug Screening Program, Contract # HHSN-271-2013-
6
7 00017-C (NIMH PDSP). The NIMH PDSP is Directed by Bryan L. Roth (mail
8
9 to:bryan_roth@med.unc.edu) at the University of North Carolina at Chapel Hill and Project
10
11 Officer Jamie Driscoll (mail to:jdrisco1@mail.nih.gov) at NIMH, Bethesda MD, USA. For
12
13 experimental details please refer to the PDSP web site <https://pdspdb.unc.edu/pdspWeb/>
14
15 (<https://pdspdb.unc.edu/pdspWeb/>).
16
17
18
19
20

21 **ABBREVIATIONS USED**

22
23
24 BBB, blood-brain barrier; VFTD, Venus flytrap domain; 7-TM, seven transmembrane; CRD
25
26 cysteine rich domain; POOL, Partial Order Optimum Likelihood; EL2, extracellular loop 2; PDB,
27
28 Protein Data Bank; PAM, positive allosteric modulator; NAM, negative allosteric modulator; MW,
29
30 molecular weight; tPSA, topological polar surface area; Cl_{int} , the intrinsic clearance; G_i , adenylate
31
32 cyclase inhibitory G-protein; MWCO, molecular weight cut off; ND, not determined; PBL, Polar
33
34 brain lipid; PBL, porcine polar brain lipid; P-gp, P-glycoprotein; PAMPA, parallel artificial
35
36 membrane permeability assay; P_e , effective permeability; EOS, end of synthesis. SWFI, sterile
37
38 water for injection; TAC, time-activity curve; SUV, standardized uptake value; USP, United States
39
40 Pharmacopeia; % ID/g, percentage of injected dose per gram of wet tissue.
41
42
43
44
45
46
47
48
49
50
51
52
53
54
55
56
57
58
59
60

REFERENCES

- (1) Tanabe, Y.; Masu, M.; Ishii, T.; Shigemoto, R.; Nakanishi, S. A family of metabotropic glutamate receptors. *Neuron* **1992**, *8*, 169-179.
- (2) Cartmell, J.; Schoepp, D. D. Regulation of neurotransmitter release by metabotropic glutamate receptors. *J. Neurochem.* **2000**, *75*, 889-907.
- (3) Gu, G.; Lorrain, D. S.; Wei, H.; Cole, R. L.; Zhang, X.; Daggett, L. P.; Schaffhauser, H. J.; Bristow, L. J.; Lechner, S. M. Distribution of metabotropic glutamate 2 and 3 receptors in the rat forebrain: Implication in emotional responses and central disinhibition. *Brain Res.* **2008**, *1197*, 47-62.
- (4) Wright, R. A.; Johnson, B. G.; Zhang, C.; Salhoff, C.; Kingston, A. E.; Calligaro, D. O.; Monn, J. A.; Schoepp, D. D.; Marek, G. J. CNS distribution of metabotropic glutamate 2 and 3 receptors: transgenic mice and [³H]LY459477 autoradiography. *Neuropharmacology* **2013**, *66*, 89-98.
- (5) Yin, S.; Noetzel, M. J.; Johnson, K. A.; Zamorano, R.; Jalan-Sakrikar, N.; Gregory, K. J.; Conn, P. J.; Niswender, C. M. Selective actions of novel allosteric modulators reveal functional heteromers of metabotropic glutamate receptors in the CNS. *J. Neurosci.* **2014**, *34*, 79-94.
- (6) Kim, S. H.; Fraser, P. E.; Westaway, D.; George-Hyslop, P. H. S.; Ehrlich, M. E.; Gandy, S. Group II metabotropic glutamate receptor stimulation triggers production and release of Alzheimer's amyloid β_{42} from isolated intact nerve terminals. *J. Neurosci.* **2010**, *30*, 3870-3875.
- (7) Richards, G.; Messer, J.; Faull, R. L. M.; Stadler, H.; Wichmann, J.; Huguenin, P.; Bohrmann, B.; Mutel, V. Altered distribution of mGlu2 receptors in β -amyloid-affected brain regions of Alzheimer cases and aged PS2APP mice. *Brain Res.* **2010**, *1363*, 180-190.

1
2
3 (8) Lee, H.-g.; Ogawa, O.; Zhu, X.; O'Neill, M. J.; Petersen, R. B.; Castellani, R. J.; Ghanbari, H.;
4 Perry, G.; Smith, M. A. Aberrant expression of metabotropic glutamate receptor 2 in the vulnerable
5 neurons of Alzheimer's disease. *Acta Neuropathol.* **2004**, *107*, 365-371.
6
7

8
9
10 (9) Caraci, F.; Molinaro, G.; Battaglia, G.; Giuffrida, M. L.; Rizzo, B.; Traficante, A.; Bruno, V.;
11 Cannella, M.; Merlo, S.; Wang, X.; Heinz, B. A.; Nisenbaum, E. S.; Britton, T. C.; Drago, F.;
12 Sortino, M. A.; Copani, A.; Nicoletti, F. Targeting group II metabotropic glutamate (mGlu)
13 receptors for the treatment of psychosis associated with Alzheimer's disease: selective activation
14 of mGlu2 receptors amplifies β -amyloid toxicity in cultured neurons, whereas dual activation of
15 mGlu2 and mGlu3 receptors is neuroprotective. *Mol. Pharmacol.* **2011**, *79*, 618-626.
16
17
18

19
20
21 (10) Moreno, J. L.; Sealfon, S. C.; Gonzalez-Maeso, J. Group II metabotropic glutamate receptors
22 and schizophrenia. *Cell. Mol. Life Sci.* **2009**, *66*, 3777-3785.
23
24
25

26
27 (11) Chaki, S. Group II metabotropic glutamate receptor agonists as a potential drug for
28 schizophrenia. *Eur. J. Pharmacol.* **2010**, *639*, 59-66.
29
30
31

32
33 (12) Downing, A. M.; Kinon, B. J.; Millen, B. A.; Zhang, L.; Liu, L.; Morozova, M. A.; Brenner,
34 R.; Rayle, T. J.; Nisenbaum, L.; Zhao, F.; Gomez, J. C. A double-blind, placebo-controlled
35 comparator study of LY2140023 monohydrate in patients with schizophrenia. *BMC Psychiatry*
36 **2014**, *14*, 351, pages 1-12.
37
38
39

40
41 (13) Patil, S.; Zhang, L.; Martenyi, F.; Lowe, S. L.; Jackson, K. A.; Andreev, B. V.; Avedisova,
42 A. S.; Bardenstein, L. M.; Gurovich, I. Y.; Morozova, M. A.; Mosolov, S. N.; Neznanov, N. G.;
43 Reznik, A. M.; Smulevich, A. B.; Tochilov, V. A.; Johnson, B. G.; Monn, J. A.; Schoepp, D. D.
44 Activation of mGluR2/3 receptors as a new approach to treat schizophrenia: a randomized Phase
45 2 clinical trial. *Nat. Med.* **2007**, *13*, 1102-1107.
46
47
48
49
50
51
52
53
54
55
56
57
58
59
60

- 1
2
3 (14) Feyissa, A. M.; Woolverton, W. L.; Miguel-Hidalgo, J. J.; Wang, Z.; Kyle, P. B.; Hasler, G.;
4
5 Stockmeier, C. A.; Iyo, A. H.; Karolewicz, B. Elevated level of metabotropic glutamate receptor
6
7 2/3 in the prefrontal cortex in major depression. *Prog. Neuro-psychoph.* **2010**, *34*, 279-283.
8
9
10 (15) Johnson, M. P.; Barda, D.; Britton, T. C.; Emkey, R.; Hornback, W. J.; Jagdmann, G. E.;
11
12 McKinzie, D. L.; Nisenbaum, E. S.; Tizzano, J. P.; Schoepp, D. D. Metabotropic glutamate 2
13
14 receptor potentiators: receptor modulation, frequency-dependent synaptic activity, and efficacy in
15
16 preclinical anxiety and psychosis model(s). *Psychopharmacology (Berl)* **2005**, *179*, 271-283.
17
18
19 (16) Mazzitelli, M.; Palazzo, E.; Maione, S.; Neugebauer, V. Group II metabotropic glutamate
20
21 receptors: role in pain mechanisms and pain modulation. *Front Mol. Neurosci.* **2018**, *11*, 383,
22
23 pages 1-11.
24
25
26 (17) Chiechio, S.; Copani, A.; Zammataro, M.; Battaglia, G.; Gereau, R. W. I. V.; Nicoletti, F.
27
28 Transcriptional regulation of type-2 metabotropic glutamate receptors: an epigenetic path to novel
29
30 treatments for chronic pain. *Trends Pharmacol. Sci.* **2010**, *31*, 153-160.
31
32
33 (18) Niswender, C. M.; Conn, P. J. Metabotropic glutamate receptors: physiology, pharmacology,
34
35 and disease. *Annu. Rev. Pharmacol. Toxicol.* **2010**, *50*, 295-322.
36
37
38 (19) Marek, G. J. When is a Proof-of-Concept (POC) not a POC? Pomaglumetad (LY2140023) as
39
40 a Case Study for Antipsychotic Efficacy. *Curr. Pharm. Des.* **2015**, *21*, 3788-3796.
41
42
43 (20) Adams, D. H.; Kinon, B. J.; Baygani, S.; Millen, B. A.; Velona, I.; Kollack-Walker, S.;
44
45 Walling, D. P. A long-term, phase 2, multicenter, randomized, open-label, comparative safety
46
47 study of pomaglumetad methionil (LY2140023 monohydrate) versus atypical antipsychotic
48
49 standard of care in patients with schizophrenia. *BMC Psychiatry* **2013**, *13*, 143, pages 1-9.
50
51
52 (21) Stauffer, V. L.; Millen, B. A.; Andersen, S.; Kinon, B. J.; Lagrandeur, L.; Lindenmayer, J. P.;
53
54 Gomez, J. C. Pomaglumetad methionil: no significant difference as an adjunctive treatment for
55
56
57
58
59
60

1
2
3 patients with prominent negative symptoms of schizophrenia compared to placebo. *Schizophr Res.*
4
5 **2013**, *150*, 434-441.

6
7 (22) Fell, M. J.; Svensson, K. A.; Johnson, B. G.; Schoepp, D. D. Evidence for the role of
8
9 metabotropic glutamate (mGlu)2 not mGlu3 receptors in the preclinical antipsychotic
10
11 pharmacology of the mGlu2/3 receptor agonist (-)-(1R,4S,5S,6S)-4-amino-2-
12
13 sulfonylbicyclo[3.1.0]hexane-4,6-dicarboxylic acid (LY404039). *J. Pharmacol. Exp. Ther.* **2008**,
14
15 *326*, 209-217.

16
17 (23) Woolley, M. L.; Pemberton, D. J.; Bate, S.; Corti, C.; Jones, D. N. C. The mGlu2 but not the
18
19 mGlu3 receptor mediates the actions of the mGluR2/3 agonist, LY379268, in mouse models
20
21 predictive of antipsychotic activity. *Psychopharmacology (Berlin, Germany)* **2008**, *196*, 431-440.

22
23 (24) Yu, M.; Nagren, K.; Chen, Y. I.; Livni, E.; Elmaleh, D.; Kozikowski, A.; Wang, X.; Jokivarsi,
24
25 K.; Brownell, A.-L. Radiolabeling and biodistribution of methyl 2-(methoxycarbonyl)-2-
26
27 (methylamino) bicyclo [2.1.1]-hexane-5-carboxylate, a potent neuroprotective drug. *Life Sci.*
28
29 **2003**, *73*, 1577-1585.

30
31 (25) Wang, J.-Q.; Zhang, Z.; Kuruppu, D.; Brownell, A.-L. Radiosynthesis of PET radiotracer as
32
33 a prodrug for imaging group II metabotropic glutamate receptors in vivo. *Bioorg. Med. Chem. Lett.*
34
35 **2012**, *22*, 1958-1962.

36
37 (26) Zhang, Z.; Brownell, A.-L. Imaging of metabotropic glutamate receptors (mGluRs). In
38
39 *Neuroimaging-clinical applications*, Bright, P., Ed. In Tech-Open Access Publisher: Rijeka,
40
41 Croatia, 2012; pp 499-532.

42
43 (27) Trabanco, A. A.; Cid, J. M.; Lavreysen, H.; MacDonald, G. J.; Tresadern, G. Progress in the
44
45 development of positive allosteric modulators of the metabotropic glutamate receptor 2. *Curr.*
46
47 *Med. Chem.* **2011**, *18*, 47-68.

1
2
3 (28) Sheffler, D. J.; Pinkerton, A. B.; Dahl, R.; Markou, A.; Cosford, N. D. P. Recent progress in
4 the synthesis and characterization of group II metabotropic glutamate receptor allosteric
5 modulators. *ACS Chem. Neurosci.* **2011**, *2*, 382-393.
6
7

8
9
10 (29) Andres, J.-I.; Alcazar, J.; Cid, J. M.; De Angelis, M.; Iturrino, L.; Langlois, X.; Lavreysen,
11 H.; Trabanco, A. A.; Celen, S.; Bormans, G. Synthesis, evaluation, and radiolabeling of new potent
12 positive allosteric modulators of the metabotropic glutamate receptor 2 as potential tracers for
13 positron emission tomography imaging. *J. Med. Chem.* **2012**, *55*, 8685-8699.
14
15
16

17
18 (30) Leurquin-Sterk, G.; Van Laere, K.; Koole, M.; Celen, S.; Bormans, G.; Langlois, X.; Te Riele,
19 P.; Schmidt Mark, E.; Van Hecken, A.; Verbruggen, A.; de Hoon, J.; Alcazar, J.; Andres, J.-I.
20 What we observe in vivo is not always what we see in vitro: development and validation of ¹¹C-
21 JNJ-42491293, a novel radioligand for mGluR2. *J. Nucl. Med.* **2017**, *58*, 110-116.
22
23
24

25
26 (31) Lohith, T.; McQuade, P.; Salinas, C.; Anderson, M.; Reynders, T.; Bautmans, A.; Bormans,
27 G.; Serdons, K.; Laere, K. V.; Hostetler, E. First-in-human PET imaging of mGluR2 receptors. *J.*
28 *Nucl. Med.* **2016**, *57*, Suppl 2:213.
29
30
31

32
33 (32) McQuade, P.; Joshi, A.; Miller, P.; Zeng, Z.; Purcell, M.; Gantert, L.; Holahan, M.; Meissner,
34 R.; Uslander, J.; Hostetler, E. Discovery and preclinical evaluation of an mGluR2-NAM PET
35 radioligand. *J. Nucl. Med.* **2016**, *57*, Suppl 2:290.
36
37
38

39
40 (33) Majo, V.; Prabhakaran, J.; Simpson, N.; Arango, V.; Mann, J. J.; Kumar, D. J. Development
41 of a [¹⁸F]-labeled positive allosteric modulator of the metabotropic glutamate receptor 2 (mGluR2)
42 as a potential PET tracer. *J. Nucl. Med.* **2013**, *54*, Suppl 2:1072.
43
44
45

46
47 (34) Ma, Y.; Kumata, K.; Yui, J.; Zhang, Y.; Yamasaki, T.; Hatori, A.; Fujinaga, M.; Nengaki, N.;
48 Xie, L.; Wang, H.; Zhang, M.-R. Synthesis and evaluation of 1-(cyclopropylmethyl)-4-(4-
49 [¹¹C]methoxyphenyl)-piperidin-1-yl-2-oxo-1,2-dihydropyridine-3-carbonitrile ([¹¹C]CMDC) for
50
51
52
53
54
55
56
57
58
59
60

PET imaging of metabotropic glutamate receptor 2 in the rat brain. *Bioorg. Med. Chem.* **2017**, *25*, 1014-1021.

(35) Kumata, K.; Yamasaki, T.; Hatori, A.; Zhang, Y.; Mori, W.; Fujinaga, M.; Xie, L.; Okubo, T.; Nengaki, N.; Zhang, M.-R. Synthesis and in vitro evaluation of three novel radiotracers for imaging of metabotropic glutamate receptor subtype 2 in rat brain. *Bioorg. Med. Chem. Lett.* **2017**, *27*, 3139-3143.

(36) Zhang, X.; Kumata, K.; Yamasaki, T.; Cheng, R.; Hatori, A.; Ma, L.; Zhang, Y.; Xie, L.; Wang, L.; Kang, H. J.; Sheffler, D. J.; Cosford, N. D. P.; Zhang, M. R.; Liang, S. H. Synthesis and preliminary studies of a novel negative allosteric modulator, 7-((2,5-Dioxopyrrolidin-1-yl)methyl)-4-(2-fluoro-4-[¹¹C]methoxyphenyl) quinoline-2-carboxamide, for imaging of metabotropic glutamate receptor 2. *ACS Chem. Neurosci.* **2017**, *8*, 1937-1948.

(37) Kumata, K.; Hatori, A.; Yamasaki, T.; Zhang, Y.; Mori, W.; Fujinaga, M.; Xie, L.; Nengaki, N.; Zhang, M. R. Synthesis and evaluation of 4-(2-fluoro-4-[¹¹C]methoxyphenyl)-5-((2-methylpyridin-4-yl)methoxy)picolinamide for PET imaging of the metabotropic glutamate receptor 2 in the rat brain. *Bioorg. Med. Chem.* **2019**, *27*, 483-491.

(38) Li, Z.; Krause, S.; Suzuki, M.; Sasaki, T. Radiotracer compounds. WO/2016033190-A1, 2016.

(39) Van Gool, M. L. M.; Andres-Gil, J. I.; Alcazar-Vaca, M. J.; Bormans, G. M. R.; Celen, S. J. L.; Joost, V. Radiolabelled mGluR2 PET ligands. WO/2016087489-A1, 2016.

(40) D'Alessandro, P. L.; Corti, C.; Roth, A.; Ugolini, A.; Sava, A.; Montanari, D.; Bianchi, F.; Garland, S. L.; Powney, B.; Koppe, E. L.; Rocheville, M.; Osborne, G.; Perez, P.; de la Fuente, J.; De Los Frailes, M.; Smith, P. W.; Branch, C.; Nash, D.; Watson, S. P. The identification of

1
2
3 structurally novel, selective, orally bioavailable positive modulators of mGluR2. *Bioorg. Med.*
4
5 *Chem. Lett.* **2010**, *20*, 759-762.

6
7
8 (41) Efremov, I. V.; Rogers, B. N.; Duplantier, A. J.; Zhang, L.; Zhang, Q.; Maklad, N. S.
9
10 Azabenzimidazolyl compounds as potentiators of mGluR2 subtype of glutamate receptor and their
11
12 preparation, pharmaceutical compositions and use in the treatment of diseases. WO/2008012622,
13
14 2008.

15
16
17 (42) Zhang, L.; Brodney, M. A.; Candler, J.; Doran, A. C.; Duplantier, A. J.; Efremov, I. V.;
18
19 Evrard, E.; Kraus, K.; Ganong, A. H.; Haas, J. A.; Hanks, A. N.; Jenza, K.; Lazzaro, J. T.; Maklad,
20
21 N.; McCarthy, S. A.; Qian, W.; Rogers, B. N.; Rottas, M. D.; Schmidt, C. J.; Siuciak, J. A.;
22
23 Tingley, F. D.; Zhang, A. Q. 1-[(1-Methyl-1H-imidazol-2-yl)methyl]-4-phenylpiperidines as
24
25 mGluR2 Positive Allosteric Modulators for the Treatment of Psychosis. *J. Med. Chem.* **2011**, *54*,
26
27 1724-1739.

28
29
30 (43) Zhang, L.; Rogers, B. N.; Duplantier, A. J.; McHardy, S. F.; Efremov, I.; Berke, H.; Qian,
31
32 W.; Zhang, A. Q.; Maklad, N.; Candler, J.; Doran, A. C.; Lazzaro, J. T.; Ganong, A. H. 3-
33
34 (imidazolylmethyl)-3-aza-bicyclo[3.1.0]hexan-6-yl)methyl ethers: a novel series of mGluR2
35
36 positive allosteric modulators. *Bioorg. Med. Chem. Lett.* **2008**, *18*, 5493-5496.

37
38
39 (44) Cid, J. M.; Tresadern, G.; Vega, J. A.; de Lucas, A. I.; del Cerro, A.; Matesanz, E.; Linares,
40
41 M. L.; Garcia, A.; Iturrino, L.; Perez-Benito, L.; Macdonald, G. J.; Oehlrich, D.; Lavreysen, H.;
42
43 Peeters, L.; Ceusters, M.; Ahnaou, A.; Drinkenburg, W.; Mackie, C.; Somers, M.; Trabanco, A.
44
45 A. Discovery of 8-trifluoromethyl-3-cyclopropylmethyl-7-[(4-(2,4-difluorophenyl)-1-
46
47 piperazinyl)methyl]-1,2,4-triazolo[4,3-a]pyridine (JNJ-46356479), a selective and orally
48
49 bioavailable mGlu2 receptor positive allosteric modulator (PAM). *J. Med. Chem.* **2016**, *59*, 8495-
50
51 8507.

- 1
2
3 (45) Krieger, E.; Joo, K.; Lee, J.; Lee, J.; Raman, S.; Thompson, J.; Tyka, M.; Baker, D.; Karplus,
4
5 K. Improving physical realism, stereochemistry, and side-chain accuracy in homology modeling:
6
7 Four approaches that performed well in CASP8. *Proteins* **2009**, *77*, 114-122.
8
9
10 (46) Kunishima, N.; Shimada, Y.; Tsuji, Y.; Sato, T.; Yamamoto, M.; Kumasaka, T.; Nakanishi,
11
12 S.; Jingami, H.; Morikawa, K. Structural basis of glutamate recognition by a dimeric metabotropic
13
14 glutamate receptor. *Nature* **2000**, *407*, 971-977.
15
16
17 (47) Dobrovetsky, E.; Khutoreskaya, G.; Seitova, A.; Cossar, D.; Edwards, A. M.; Arrowsmith, C.
18
19 H.; Bountra, C.; Weigelt, J.; Bochkarev, A. Ligand binding domain of metabotropic glutamate
20
21 receptor mGluR5 complexed with glutamate. RCSB Protein Data Bank, 2017,
22
23 DOI:10.2210/pdb3LMK/pdb
24
25
26 (48) Koehl, A.; Hu, H. L.; Feng, D.; Sun, B. F.; Zhang, Y.; Robertson, M. J.; Chu, M.; Kobilka,
27
28 T. S.; Laermans, T.; Steyaert, J.; Tarrasch, J.; Dutta, S.; Fonseca, R.; Weis, W. I.; Mathiesen, J.
29
30 M.; Skiniotis, G.; Kobilka, B. K. Structural insights into the activation of metabotropic glutamate
31
32 receptors. *Nature* **2019**, *566*, 79-84.
33
34
35 (49) McGuffin, L. J.; Shuid, A. N.; Kempster, R.; Maghrabi, A. H. A.; Nealon, J. O.; Salehe, B.
36
37 R.; Atkins, J. D.; Roche, D. B. Accurate template-based modeling in CASP12 using the IntFOLD4-
38
39 TS, ModFOLD6, and ReFOLD methods. *Proteins* **2018**, *86*, 335-344.
40
41
42 (50) Waterhouse, A.; Bertoni, M.; Bienert, S.; Studer, G.; Tauriello, G.; Gumienny, R.; Heer, F.
43
44 T.; de Beer, T. A. P.; Rempfer, C.; Bordoli, L.; Lepore, R.; Schwede, T. SWISS-MODEL:
45
46 homology modelling of protein structures and complexes. *Nucleic Acids Res.* **2018**, *46*, W296-
47
48 W303.
49
50
51 (51) Eisenberg, D.; Luthy, R.; Bowie, J. U. VERIFY3D: assessment of protein models with three-
52
53 dimensional profiles. *Methods Enzymol.* **1997**, *277*, 396-404.
54
55
56
57
58
59
60

1
2
3 (52) Colovos, C.; Yeates, T. O. Verification of protein structures: patterns of nonbonded atomic
4 interactions. *Protein Sci.* **1993**, *2*, 1511-1519.

7 (53) Tong, W. X.; Wei, Y.; Murga, L. F.; Ondrechen, M. J.; Williams, R. J. Partial Order Optimum
8 Likelihood (POOL): Maximum likelihood prediction of protein active site residues using 3D
9 structure and sequence properties. *PLoS Comput. Biol.* **2009**, *5*, 1-15.

14 (54) Tan, K. P.; Varadarajan, R.; Madhusudhan, M. S. DEPTH: a web server to compute depth
15 and predict small-molecule binding cavities in proteins. *Nucleic Acids Res.* **2011**, *39*, W242-W248.

19 (55) Huang, B. D. MetaPocket: A meta approach to improve protein ligand binding site prediction.
20 *OMICS* **2009**, *13*, 325-330.

24 (56) Morris, G. M.; Goodsell, D. S.; Halliday, R. S.; Huey, R.; Hart, W. E.; Belew, R. K.; Olson,
25 A. J. Automated docking using a Lamarckian genetic algorithm and an empirical binding free
26 energy function. *J. Comput. Chem.* **1998**, *19*, 1639-1662.

31 (57) Perez-Benito, L.; Doornbos, M. L. J.; Cordomi, A.; Peeters, L.; Lavreysen, H.; Pardo, L.;
32 Tresadern, G. Molecular switches of allosteric modulation of the metabotropic glutamate 2
33 receptor. *Structure* **2017**, *25*, 1153-1162.

37 (58) Doornbos, M. L. J.; Cid, J. M.; Haubrich, J.; Nunes, A.; van de Sande, J. W.; Vermond, S. C.;
38 Mulder-Krieger, T.; Trabanco, A. A.; Ahnaou, A.; Drinkenburg, W. H.; Lavreysen, H.; Heitman,
39 L. H.; AP, I. J.; Tresadern, G. Discovery and kinetic profiling of 7-aryl-1,2,4-triazolo[4,3-
40 a]pyridines: positive allosteric modulators of the metabotropic glutamate receptor 2. *J. Med. Chem.*
41 **2017**, *60*, 6704-6720.

48 (59) Doornbos, M. L.; Perez-Benito, L.; Tresadern, G.; Mulder-Krieger, T.; Biesmans, I.;
49 Trabanco, A. A.; Cid, J. M.; Lavreysen, H.; AP, I. J.; Heitman, L. H. Molecular mechanism of
50
51
52
53
54
55
56
57
58

1
2
3 positive allosteric modulation of the metabotropic glutamate receptor 2 by JNJ-46281222. *Br. J.*
4
5 *Pharmacol.* **2016**, *173*, 588-600.

6
7 (60) Poutiainen, P.; Kil, K. E.; Zhang, Z.; Kuruppu, D.; Tannous, B.; Brownell, A.-L. Co-operative
8
9 binding assay for the characterization of mGlu4 allosteric modulators. *Neuropharmacology* **2015**,
10
11 *97*, 142-148.

12
13 (61) Kil, K. E.; Poutiainen, P.; Zhang, Z.; Zhu, A.; Choi, J. K.; Jokivarsi, K.; Brownell, A.-L.
14
15 Radiosynthesis and evaluation of an ¹⁸F-labeled positron emission tomography (PET) radioligand
16
17 for metabotropic glutamate receptor subtype 4 (mGlu4). *J. Med. Chem.* **2014**, *57*, 9130-9138.

18
19 (62) Roth, B. L. Assay protocol book. In Version III ed.; PDSP, N., Ed. Department of
20
21 Pharmacology, University of North Carolina at Chapel Hill, 2018.

22
23 (63) DiRaddo, J. O.; Miller, E. J.; Hathaway, H. A.; Grajkowska, E.; Wroblewska, B.; Wolfe, B.
24
25 B.; Liotta, D. C.; Wroblewski, J. T. A real-time method for measuring cAMP production
26
27 modulated by G $\alpha_{i/o}$ -coupled metabotropic glutamate receptors. *J. Pharmacol. Exp. Ther.* **2014**,
28
29 *349*, 373-382.

30
31 (64) Jin, X.; Semenova, S.; Yang, L.; Ardecky, R.; Sheffler, D. J.; Dahl, R.; Conn, P. J.; Cosford,
32
33 N. D. P.; Markou, A. The mGluR2 positive allosteric modulator BINA decreases cocaine self-
34
35 administration and cue-induced cocaine-seeking and counteracts cocaine-induced enhancement of
36
37 brain reward function in rats. *Neuropsychopharmacol.* **2010**, *35*, 2021-2036.

38
39 (65) Minick, D. J.; Frenz, J. H.; Patrick, M. A.; Brent, D. A. A comprehensive method for
40
41 determining hydrophobicity constants by reversed-phase high-performance liquid
42
43 chromatography. *J. Med. Chem.* **1988**, *31*, 1923-1933.

44
45 (66) Pike, V. W. PET radiotracers: crossing the blood-brain barrier and surviving metabolism.
46
47 *Trends Pharmacol. Sci.* **2009**, *30*, 431-440.

1
2
3 (67) Banker, M. J.; Clark, T. H.; Williams, J. A. Development and validation of a 96-well
4 equilibrium dialysis apparatus for measuring plasma protein binding. *J. Pharm. Sci.* **2003**, *92*, 967-
5
6
7
8 974.

9
10 (68) Di, L.; Kerns, E. H.; Hong, Y.; Chen, H. Development and application of high throughput
11 plasma stability assay for drug discovery. *Int. J. of Pharm.* **2005**, *297*, 110-119.

12
13 (69) Houston, J. B. Utility of in vitro drug metabolism data in predicting in vivo metabolic
14 clearance. *Biochem. Pharmacol.* **1994**, *47*, 1469-1479.

15
16 (70) Engers, D. W.; Niswender, C. M.; Weaver, C. D.; Jadhav, S.; Menon, U. N.; Zamorano, R.;
17
18
19
20
21
22
23
24
25
26
27
28
29
30
31
32
33
34
35
36
37
38
39
40
41
42
43
44
45
46
47
48
49
50
51
52
53
54
55
56
57
58
59
60
Conn, P. J.; Lindsley, C. W.; Hopkins, C. R. Synthesis and evaluation of a series of
heterobiaryl amides that are centrally penetrant metabotropic glutamate receptor 4 (mGluR4)
positive allosteric modulators (PAMs). *J. Med. Chem.* **2009**, *52*, 4115-4118.

(71) Kil, K.-E.; Zhang, Z.; Jokivarsi, K.; Gong, C.; Choi, J.-K.; Kura, S.; Brownell, A.-L.
Radiosynthesis of *N*-(4-chloro-3-[¹¹C]methoxyphenyl)-2-picolinamide ([¹¹C]ML128) as a PET
radiotracer for metabotropic glutamate receptor subtype 4 (mGlu₄). *Bioorg. Med. Chem.* **2013**, *21*,
5955-5962.

(72) Di, L.; Kerns, E. H.; Chen, H.; Petusky, S. L. Development and application of an automated
solution stability assay for drug discovery. *J. Biomol. Screen.* **2006**, *11*, 40-47.

(73) Di, L.; Kerns, E. H.; Fan, K.; McConnell, O. J.; Carter, G. T. High throughput artificial
membrane permeability assay for blood-brain barrier. *Eur. J. Med. Chem.* **2003**, *38*, 223-232.

(74) Promega. Pgp-Glo Assay System, Instructions for use of products V3591 and V3601. In
Technical bulletin, Promega: 2015.

1
2
3 (75) Altschul, S. F.; Madden, T. L.; Schaffer, A. A.; Zhang, J. H.; Zhang, Z.; Miller, W.; Lipman,
4 D. J. Gapped BLAST and PSI-BLAST: a new generation of protein database search programs.

5
6
7
8 *Nucleic Acids Res.* **1997**, *25*, 3389-3402.

9
10 (76) Hanwell, M. D.; Curtis, D. E.; Lonie, D. C.; Vandermeersch, T.; Zurek, E.; Hutchison, G. R.
11 Avogadro: an advanced semantic chemical editor, visualization, and analysis platform. *J.*

12
13
14
15 *Cheminformatics.* **2012**, *4*, 1-17.
16
17
18
19
20
21
22
23
24
25
26
27
28
29
30
31
32
33
34
35
36
37
38
39
40
41
42
43
44
45
46
47
48
49
50
51
52
53
54
55
56
57
58
59
60

Table of Contents Graphic

